AD-757 941

HIGH SPEED WATER JETS FROM VERTICALLY ACCELERATED ROTATING CONES

P. Savic, et al

National Research Council of Canada
Ottawa, Ontario

December 1972

DISTRIBUTED BY:

NTIS

National Technical Information Service
U. S. DEPARTMENT OF COMMERCE
5285 Port Royal Road, Springfield Va. 22151

National Research Council Canada

Conseil national de recherches Canada

MECHANICAL ENGINEERING REPORT

MD-72

HIGH SPEED WATER JETS FROM VERTICALLY ACCELERATED ROTATING CODES

Reproduced by
NATIONAL TECHNICAL
INFORMATION SERVICE
U.S. Department of Commerce
Springfield, VA 22151

HIGH SPEED WATER JETS FROM VERTICALLY ACCELERATED ROTATING CONES

by

P. SAVIC, J.D. ALLAN AND G.P. Van BLOKLAND

Details of illustrations in this document may be better studied on microfiche.

APR 9 1973

A.J. Bachmeier, Head
Gas Dynamics Section

D.C. MacPhail
Director

ABSTRACT

Water jets are produced by vertically accelerating a rotating cone partially filled with water. It is shown that the acceleration of the parabolic meniscus results in a motion similar to that observed in a shaped explosive charge. (Monroe jet). Acceleration of the cone is effected by means of an inductive electromagnetic accelerating device (conical pinch) whose theory is developed in terms of the WKB approximation. A second order inviscid theory is presented of the motion of the fluid in the cone in terms of the Penney-Price linearization procedure and it is shown that good agreement for the jet head velocity can be achieved for low velocities. At higher velocities, experimental results appear to lag behind theory, probably owing to the dispersal of the jet head through viscous drag with the surrounding atmosphere. The shape of the jet at early times is well represented by first order theory.

TABLE OF CONTENTS

ILLUSTRATIONS

ILLUSTRATIONS (Cont'd)

HIGH SPEED WATER JETS FROM VERTICALLY ACCELERATED ROTATING CONES

1.0 INTRODUCTION

High speed water jets have for some time been used for drilling, cutting and shaping various materials. The advantages of this technique lie in the small width of attainable cuts and the avoidance of the necessity to sharpen the work tool. Since most methods of water jet production comprise of high-pressure pump followed by pipes, nozzles and possibly hydraulic intensifiers, the maximum stagnation pressures attainable in the jets depends on the strength of the walls used to enclose the hydraulic circuit. To overcome this limitation, it has been suggested that some form of hydrodynamic jet intensification involving converging flow may be used. One such device is the Monroe jet or shaped charge. In this case an explosive charge containing a conical hole lined with a layer of metal is exploded at the end nearest the apex of the cone. The resulting detonation wave compresses the metal lining, causing it to flow towards the centre line and along it to form a narrow jet of considerable speed and penetrating power. The theory of this mechanism has been fully explored and tested experimentally[1-4]. As the jet is free-standing it does not require confining walls and hence the problem of wall strength does not arise. Obviously the repeatability of such a device is severely limited by the fact that the source of the jet is totally destroyed in the process. For this reason the suggestion has been made that the explosive charge be replaced by a magnetic compression device and the metal lining by some sort of liquid film. That magnetic pressures of great magnitude can be generated has recently been shown by Bless[5]. It remains to couple the magnetic force in some way to the liquid film. Preliminary experiments in this laboratory, using a layer of mercury indicate that the liquid becomes unstable under an external magnetic field and no jet is formed. Further experiments using non-conducted fluids contained in a deformable hollow metal cone were equally unsuccessful, as the cone became subject to elastic instability, except in the case of small strain, as will be further discussed below.

As the theory of the Monroe jet uses nothing but ideal incompressible and inviscid fluid characteristics, it may be argued that a cone lined with a liquid layer and accelerated along its axis is in fact equivalent to a cone that collapses in a manner in which all points on the cone wall approach the centre line with equal velocity, the only difference being that in the former case an additional shear velocity along the cone wall is imposed, which, since the liquid is assumed inviscid, does not alter the mechanics of the motion. This is the solution adopted in this work, whereby the liquid layer is produced by rotating the cone about its axis. It will be shown in the following that, although the liquid layer produced in this way is by no means of uniform thickness, the velocity amplification of the resulting jet relative to the cone is considerable and in the case of the meniscal parabola being tangent to the cone, corresponds to the findings of the Monroe jet theory.

2.0 ELECTROMAGNETIC ACCELERATION OF A CONE

The theory of the "electromagnetic cannon" or accelerator has been extensively considered[6,7], among others by Mostov et.al.[7] who present probably the most complete

and elegant treatment. We shall here reproduce some of the basic equations but then resort to an analytical approximation involving the WKB scheme, rather than consider asymptotic and power-series solutions as in Reference 7. The analytical foundations of the WKB method have been well documented [8] and we shall show by means of comparison with analog solutions that it yields results of adequate accuracy in the present case also. We depart from the treatment in Reference 7 not only in the method but also in the fact that for practical reasons we have to take account of the fact that the inductance of the circuit is not a linear function of the displacement of the load.

We consider at first a circuit made up of a condenser of capacity c charged to a voltage V_o followed by a circuit resistance R and in inductance L. The metallic cone is thought to be imbedded in the coil whose inductance is a linear function of the axial displacement x of the cone, i.e.

$$L = L_o + x.dL/dx = L_o + xL_1 \tag{1}$$

The quantity of greatest interest will be the transfer efficiency ϵ, which is the ratio of the kinetic energy imparted to the cone of mass m to the energy initially stored in the condenser. It can be shown that the magnetic force F_B driving the cone is given by:

$$F_B = L_1 i^2/2$$

where i is the instantaneous current in the circuit. Hence, we have the circuit equation:

$$\frac{d^2}{dt^2}(Li) + R\frac{dI}{dt} + i/c = 0 \tag{2}$$

and the force balance equation:

$$m.\frac{d^2x}{dt^2} = L_1 i^2/2 \tag{3}$$

The relations (1)-(3) form a system of equations which completely describe the motion provided a suitable set of initial conditions is imposed. To find the transfer efficiency we shall however employ the energy relation directly. If the velocity of the cone is denoted by v, we have from energy balance:

$$V_o^2 c/2 = R \int i^2 dt + mv^2/2$$

indicating balance between condenser energy, kinetic energy of the cone and ohmic heat dissipation. Integrating (3), we obtain:

$$m.v = 1/2L_1 \int i^2 dt$$

Eliminating the integral between these two relations, we obtain a quadratic relation in v. Solving in terms of the transfer efficiency:

$$\epsilon = mv^2/cV_o^2 = \frac{2mR^2}{EL_1^2}\left[1 - (1 + EL_1^2/2mR^2)^{1/2}\right]^2 \qquad (4)$$

where $E = V_o^2 c/2$ is the condenser energy. In this treatment it is assumed that the circuit resistance is independent of the position of the cone, an assumption which is usually borne out in practice, where the external losses in the conductors and the condenser dielectric predominate over the losses in the cone. An even simpler expression for the transfer efficiency can be obtained by introducing a velocity characteristic of the electromechanical circuit, the "circuit speed":

$$C = R/2L_1 \qquad (5)$$

Though this expression is only a symbolic velocity, it can be shown[9] that by means of it the equation governing the motion of the driven gas in an electromagnetic shock tube can be rendered in a form exactly analogous to that of the gas-driven shock tube (Taub's equation), where C then corresponds to the sound velocity of the undisturbed gas. Correspondingly, one can define a "circuit Mach number":

$$M = v/C$$

in terms of which the transfer efficiency becomes:

$$\epsilon = M/(M + 8) \qquad (6)$$

Within the assumptions made, Equations (4) and (6) are exact; however for the sake of the generalization made in the following it will be useful to attempt an approximate treatment based on the WKB scheme. This will enable us not only to calculate the transfer efficiency for the more general case of the inductance not being a linear function of the cone displacement, but also to study the motion and the development of the electrical quantities with the passage of time. It is convenient to first transform the relevant equations into non-dimensional units, thus:

$$T = t/(cL_o)^{1/2}, \quad Z = xL_1/L_o, \quad K = R.(c/L_o)^{1/2}, \quad Y = iL_1(c/2m)^{1/2} \qquad (7)$$

Eliminating L between (1) and (2), one can now write (2) and (3) in the form:

$$\frac{d^2}{dT^2} Y(1 + Z) + K \frac{dY}{dT} + Y = 0 \tag{8}$$

$$\frac{d^2Z}{dT^2} = Y^2 \tag{9}$$

The following initial and boundary conditions apply:

$$\left.\begin{aligned} Y &= 0 \\ Y' &= P \\ Z &= 0 \\ Z' &= 0 \end{aligned}\right\} \quad \text{when } T = 0$$

$$Y \to 0 \quad \text{as } T \to \infty \tag{10}$$

where primes denote differentiation with respect to T. From the electrical conditions at T = 0 it follows that:

$$P = V_o c L_1 / (2m L_o)^{1/2} \tag{11}$$

To eliminate the first-order term in (8) we set:

$$Y = (1 + Z)^{-1} . g(T) . \exp.(- \frac{K}{2} . \int \frac{dT}{1 + Z})$$

where g(T) is an unknown function of T. One obtains from (8):

$$g'' + g(1 + Z)^{-2}(1 + Z - \frac{KZ'}{2} - \frac{K^2}{4}) = 0 \tag{12}$$

This is now in a form suitable for application of the WKB technique. One obtains approximately:

$$g = \frac{\sin \int \left[(1 + Z)^{-1} + (1 + Z)^{-2} (-KZ'/2 - K^2/4) \right]^{1/2} dT}{\left[(1 + Z)^{-1} + (1 + Z)^{-2} (-KZ'/2 - K^2/4) \right]^{1/4}} \tag{13}$$

Since both K and Z are smaller than unity in practice and as the denominator in (13) is raised to a small power, we retain only the first term therein. Hence, (9) can be written in terms of (13):

$$\frac{d^2Z}{dT^2} = \frac{P^2}{2(1 + Z)^{3/2}} \quad (1 - \cos 2U) . \exp . \left(-K \int \frac{dT}{1 + Z}\right) \tag{14}$$

where U is the argument of the sine in (13). To determine the final velocity of the cone, (14) will be integrated from 0 to infinity. The oscillatory term contributes very little and can be neglected. Furthermore, in accordance with the third and fourth initial conditions (10) we assume:

$$Z = q^2 T^2 \tag{15}$$

where q is an as yet undetermined constant. Changing the independent variable as follows:

$$qT = \tan \delta$$

we obtain for the integral of (14):

$$(Z')_\infty = \frac{P^2}{2q} \int_0^{\pi/2} \cos \delta . \exp . (-kq^{-1} \delta) . d\delta$$

which can be evaluated to give:

$$(Z')_\infty = \frac{P^2}{2q} \left[K/q + \exp . (-K\pi/2q) \right] . (1 + K^2/q^2)^{-1} \tag{16}$$

from which the transfer efficiency can be determined as follows:

$$(Z')^2/P^2 = 2\epsilon = \frac{P^2}{4q^2} . \left[K/q + \exp . (-K\pi/2q) \right]^2 . (1 + K^2/q^2)^{-2} \tag{17}$$

The constant q is now determined by considering that as the loss factor K vanishes, the efficiency must approach unity. It follows that $q = P.(8)^{-1/2}$.

It appears from (17) that the transfer efficiency is a function of P/K, as indeed it must according to (4). Moreover, comparison of the exact expression (4) with the approximation (17) in Figure 1 shows that agreement is good over most of the range of the function. Also shown in Figure 1 are the points obtained from the solution of the system (8) - (10) by means of an analog computer. The agreement is good except for low values of K where the available integration time is insufficient to yield a final constant value for the efficiency.

Further comparison between the analog and the WKB solutions was attempted by determining the value of T for which the current Y passes through zero. This value was determined graphically from the analog solution and compared with the WKB solution (13) and (15). The comparison is shown in Figure 2 where it can be seen that the agreement is adequate for the greater part of the range of the parameters and variables involved.

It follows from Equation (4) and Figure 1 that the efficiency can be kept as close to unity as desired provided the condenser voltage is chosen high enough. Physically this may be interpreted to mean, that the velocity with which the cone leaves the coil determines the fraction of the total energy which goes into ohmic loss; if this velocity is high, the time available for creation of this loss is short compared with the time taken to accelerate the cone to its final speed.

A much more serious limitation on the efficiency attainable is imposed by the fact that in practice it is difficult to achieve a configuration of electromagnetic accelerator in which the inductance is a strictly linear function of the load displacement. In the present case, measurement of the variable inductance with the aid of an impedance bridge showed a functional dependence closely following that of a negative exponential (Fig. 3). We shall show in the following to what extent the previous analysis must be modified to take account of the non-linear behaviour of the circuit inductance.

2.1 Non-Linear Change of Inductance with Load Displacement

From the above mentioned inductance measurements it appears that the dependence of the total circuit inductance on the load displacement can be represented by:

$$L = L_o + \frac{L_1}{d} \left[1 - \exp.(-dx) \right]$$

or in terms of the non-dimensional parameters (Q):

$$L = L_o \left[1 + Q^{-1} \left(1 - \exp.(-QZ) \right) \right] \tag{18}$$

where

$$Q = L_o d / L_1 \tag{19}$$

is the non-dimensional inductance coefficient. Putting:

$$1 + Q^{-1}\left[1 - \exp.(-QZ)\right] = f(Z)$$

we note that (8) remains unchanged except that f(Z) is substituted for 1 + Z. In (9), however, we must replace L_1 by the more general term dL/dx, whence we obtain:

$$\frac{d^2Z}{dT^2} = Y^2.\exp.(-QZ) \tag{20}$$

Proceeding as before by utilizing the WKB technique, we obtain:

$$\frac{d^2Z}{dT^2} = 2^{-1}P^2f^{-3/2}\exp.(-QZ - K\int f^{-1}dT) \tag{21}$$

From this, the maximum transfer efficiency ϵ_{max} can be derived at once. We note first that as K = 0, the differential Equation (21) does not contain T explicitly; one may therefore put:

$$\frac{dZ}{dT} = p, \quad \frac{d^2Z}{dT^2} = 1/2\,\frac{dp^2}{dT}$$

and hence the limiting velocity p_m is given by:

$$p_m^2 = -P^2Q^{-1}\int_0^{\infty}(1 + Q^{-1} - Q^{-1}\exp.(-QZ))^{-3/2}\,d(\exp.-QZ)$$

from which follows that:

$$P^{-2}p_m^2 = 2\epsilon_{max} = 2\left(1 - \sqrt{\frac{Q}{Q+1}}\right) \tag{22}$$

It will be seen from (22) that, contrary to the linear case, the maximum efficiency can no longer be made as close to unity as desired. Figure 4 shows that the efficiency drops away from unity to zero as Q varies from 0 to infinity.

Of greater practical interest is the general case where K does not vanish. An approximate solution may be obtained using the same variable substitution as in 2.0. We derive:

$$\epsilon = \left[\int_0^{\pi/2}\cos\delta.\exp.(-Kq^{-1}\delta - Q\tan^2\delta)\;d\delta\right]^2 \tag{23}$$

where q is again given by $P.(8)^{-1/2}$. This integral may be evaluated explicitely by approximating $\exp.(-Q.\tan^2\delta)$ by an even-term Fourier series of three terms, thus:

$$\exp.(-Q.\tan^2\delta) = a_o + a_2\cos 2\delta + a_4\cos 4\delta$$

where

$$a_n = 4.\pi^{-1}\int_o^{\pi/2} \cos n\delta.\exp.(-Q.\tan^2\delta)\ d\delta$$

It is convenient to transform these integrals into those involving only powers of the cosine, thus:

$$b_n = \int_o^{\pi/2} \cos^{2n}\delta.\exp.(-Q\tan^2\delta).d\delta = 1/2 \int_o^{\infty} u^{-1/2}\,(1+u)^{-n-1}\exp.(-Qu)\,du$$

The last integral on the right may be expressed in terms of confluent hypergeometric functions which in this case reduce[10] to combinations of square roots, exponentials and error functions. Finally it remains to evaluate integrals involving products of exponentials and cosines, the result of which is easily obtained[11].

Results of these calculations are shown in Figure 5, where it is seen that the efficiency in each curve reaches a saturation value which cannot be exceeded no matter how large the driving energy. As an additional check, the saturation efficiencies were plotted in Figure 4 and compared with the simpler formula (22). It is seen that although the three-term Fourier series is a rather rough approximation, the agreement is fair.

In conclusion of this chapter we shall derive one additional formula which has proved particularly useful in the comparison of theory and experiment. In most of our experiments the ratio P/K was quite large. The first exponential in (23) will therefore reduce to small values for small δ. It is therefore admissible to replace the cosine by unity and $\tan\delta$ by δ^2, obtaining:

$$\epsilon = \left[\int_o^{\infty} \exp.(-K.q^{-1}\delta - Q\delta^2)\ d\delta\right]^2$$

The same restrictions imposed on the variables also permits us to replace the upper integration limit by infinity. The integral can be evaluated using known formulas[12] yielding:

$$\epsilon = \pi\,(4Q)^{-1}\left[\exp.(w^{-1}).\mathrm{erfc}(w^{-1/2})\right]^2$$

where:

$$w = P^2Q/2K^2$$

Further, if w is small, the asymptotic limit of the error function complement may be used, giving:

$$\epsilon = \frac{w}{4} (1 - Qw) \tag{24}$$

In Figure 6 experimental efficiencies were compared with calculated ones using (24). The agreement is seen to be quite good. The experimental techniques used in obtaining the measured values will be discussed below.

In the foregoing it has been assumed that the mass of the cone plus the virtual mass of the liquid contained are independent of the speed and acceleration, which is generally the case.

3.0 HYDRODYNAMICS OF JET FORMATION

3.1 Stability of Rotating Liquid in a Cone

If a circular cone partially filled with liquid is rotated about its axis, the meniscus of the liquid rises to form a paraboloidal free surface. Contrary to what occurs in a vessel with cylindrical sides, this process cannot be continued to ever-increasing rotational speeds. When this speed reaches a value at which the paraboloid becomes tangent to the side of the cone, the liquid becomes unstable and spills over the edge of the cone. Thus the limit to which a liquid layer can be created in this manner is imposed by the existence of a critical rotational speed. We shall calculate this speed from simple geometrical considerations.

Figure 7 shows the cross section of a half-cone with apex angle θ_o. The height of the liquid at zero rotational speed is H_o and the radius of its meniscus R_o. When rotated it rises to a height of H_1 and a radius of R_1. Pressure balance at the paraboloidal meniscus demands that the meniscus assumes a shape given by:

$$g(H_1 - r_1 - z) = 1/2\,\Omega^2(y^2 - R_1^2)$$

Volume integration shows that the volume of the liquid is:

$$\frac{R_1^2 \pi H_1}{3} - \frac{R_1^4 \pi \Omega^2}{4g}$$

where Ω is the angular velocity and g the acceleration of gravity. This volume must equal the volume of the unrotated liquid:

$$\frac{R_o^2 \pi H_o}{3}$$

In addition we have from geometrical considerations:

$$\tan \theta_o = R_1/H_1 = R_o/H_o$$

From this and the volume balance equation we obtain:

$$R_1^4 - 4gR_1^3.\cot \theta_o/3\Omega^2 + 4R_o^3 g \cot \theta_o/3\Omega^2 = 0$$

This quartic equation in R_1 has the form:

$$X^4 - MX^3 + N = 0$$

The meniscus is tangent to the cone provided that this equation has two coinciding roots, the condition for which is:

$$27M^4 = 256N$$

from which is obtained the critical rotational speed Ω^*:

$$\Omega^* = 2^{-1/3} \cot \theta \, .(g/H_o)^{1/2} \qquad (25)$$

This relation is shown graphically in Figure 8 where the critical speed is plotted against the initial depth $h = H_1 - H_o$. Also shown are experimental points obtained with water and mercury. The agreement may be considered fair in view of the presence of capillary effects and the difficulty in determining the exact point of criticality.

3.2 Jet Formation Under Artificial Gravity

We shall here diverge somewhat from the classical theory of Monroe jet formation, as in our case the liquid layer is not of uniform thickness. An observer moving with the cone will conclude that the meniscus is the proper equilibrium shape between the actions of gravitation and centrifugal force. As the cone accelerates upward, the observer will experience a sudden increase of apparent gravity and will rightly conclude that the meniscus must assume a different shape. The unsteady motion of this readjustment will cause a jet to develop near the trough of the meniscus which will rapidly move ahead of the edge of the cone. How this motion is influenced by the rotational speed and the filling level of the cone will be analyzed in the following.

Since for practical reasons the interest centers mainly on a knowledge of the velocity of the head of the jet, much valuable information can be gathered from a linearized

analysis. The full problem involving the non-linear terms in the equations of hydrodynamics as well as considerations of a free surface of ever-changing shape requires extensive numerical study and will therefore not be considered here. On the other hand Penney and Thornhill[13] have shown that a linearized treatment with initially fixed surfaces may yield valuable information relating to such problems as the collapse of a fluid column under gravity. The approach will be adopted in the following. The fluid in the cone is considered ideal, inviscid and incompressible and, while the paraboloidal meniscus is formed by rotational effects, all further influence of rotations on the motion is neglected. This latter assumption may be subject to revision in certain cases, as will be shown below.

The essence of the method of Penney et.al. lies in the neglect of the velocity convection terms in Euler' equation, together with considering the free surface to be acted upon by the hydrostatic pressure of the fluid column above the lowest point. The fluid adjacent to the other bounding surfaces are subject to the usual conditions of vanishing transverse flow. If all surfaces involved are members of the same orthogonal set of co-ordinate surfaces, the problem is solved at once by the method of eigenfunctions expansion. Though unfortunately the paraboloidal meniscus and the conical container do not belong to the same co-ordinate system, a two-step approximation procedure has been adopted which was found to give useful information of the motion for the case where the distortion of the free surface is not too great. However, to permit this last step, it is necessary to make the additional assumption that the cone is slender, i.e. that its apex angle is small.

3.2.1 First Order Approximation

We adopt a spherical polar co-ordinate system as depicted in Figure 7. We seek a solution of Laplace's equation for the velocity potential ϕ subject to the boundary conditions:

$$\frac{\partial \phi}{\partial \theta} = 0 \quad \text{for } \theta = \theta_o$$

$$\left(\frac{\partial \phi}{\partial t}\right)_{\text{free surface}} = p/\rho = z.dV/dt \tag{26}$$

The first of these conditions expresses the fact that no flow exists across the surface of the cone. The second, in which p is the pressure, ρ the density and V the vertical velocity of the cone derives from the condition of Penney et.al. that the pressure on the free surface is equal the hydrostatic pressure due to the height of the fluid above the parabolic trough*. In the first order, the free surface is defined as $r = r_1$. This is in accordance with the assumption that the cone is slender and that the constant radius vector describes an essentially plane surface. The general solution of Laplace's equation can be written thus:

$$\phi = \sum A_n (r/R_1)^n . P_n(\cos \theta)$$

---

* It is assumed that dV/dt is much larger than g.

where A_n are undetermined constants and P_n are Legendre functions. Since θ_o is assumed small, all the running indices (which may be non-integer) will be large. It is therefore permissible to substitute the asymptotic Bessel function representation for the Legendre functions, thus:

$$P_n(\cos\theta) \cong J_o\left[(n + 1/2)\theta\right]$$

to obtain:

$$\phi = \sum A_n (r/H_1)^{q_n/\theta_o - 1/2} J_o(q_n\theta/\theta_o) \tag{27}$$

where q_n are the zeros of the Bessel function $J_1(q_n) = 0$. Writing the equation of the parabolic surface in Figure 7 as:

$$z = \gamma y^2 \quad \text{where } \gamma = \Omega^2/2g$$

we see that:

$$(z/\gamma)^{1/2} = (r_1 + z).\tan\theta \cong (r_1 + z).\theta$$

where the tan has been replaced by its argument in accordance with the slender cone assumption. Solving for z to second order:

$$z \cong \gamma\theta^2 r_1^2$$

obtaining for the second condition (26):

$$\left(\frac{\partial\phi}{\partial t}\right)_{\text{free surface}} = \gamma\theta^2 r_1^2 . dV/dt$$

Integrating with respect to t,

$$\phi_{r = R_1} = \gamma V \theta^2 r_1^2 \tag{28}$$

This is the final form of the second boundary condition (26). Together with (27) we therefore have:

$$\sum A_n . J_o(q_n \theta/\theta_o) = \gamma V \theta_o^2 r_1^2 . (\theta/\theta_o)^2$$

This is Dini's form of a Fourier-Bessel expansion which can be solved immediately by employing the series representation:

$$\sum J_o(q_n x) . q_n^{-2} / . J_o(q_n) = x^2/4$$

from which follows that the coefficients of the series are:

$$A_n = 4V \gamma \theta_o^2 r_1^2 q_n^{-2} / J_o(q_n)$$

To determine the velocity components on the free surface, we remember that:

$$v_r = \partial \phi / \partial r, \quad v_\theta = \partial \phi / (r . \partial \theta)$$

whence on the free surface:

$$\begin{aligned} v_r &= 4V \gamma \theta_o r_1 . F(\theta/\theta_o) \\ v_\theta &= 2V \gamma \theta_o r_1 (\theta/\theta_o) \end{aligned} \tag{29}$$

The function F(x) is the sum of the series:

$$F(x) = \sum J_o(q_n x) . q_n^{-1} / J_o(q_n) \tag{30}$$

where the term -1/2 has been neglected relative to the much larger values of q_n/θ_o.

3.2.2 Approximate Summation of the Series F(x)

With (29) the problem of the first-order solution is formally solved; however, the series (30) is cumbersome and converges slowly. We shall attempt an approximate summation of this series in finite terms. Since q_n are large numbers, it is admissible to represent $J_o(q_n)$ in terms of its asymptotic value:

$$J_o(q_n) \cong (2/\pi q_n)^{1/2} \cos (q_n - \pi/4) \tag{31}$$

and as approximately:

$$q_n \cong \pi (n + 1/4)$$

it follows that (30) may be written as:

$$F(x) = (\pi / 2) \sum J_o(q_n x) . J_o(q_n)$$

On the other hand we have:

$$J_o(\pi n) = (\pi)^{-1} (2/n)^{1/2} \cos (\pi n - \pi / 4) = n^{-1/2}/\pi$$

substituting in (31) for $q_n = \pi (n + 1/4)$ it appears that on neglecting 1/4 under the square root, there results:

$$J_o(\pi n) \cong 2^{-1/2} J_o(q_n) \qquad (32)$$

If in (30) the argument $q_n x$ is replaced by $x \pi (n + 1/4)$ and the addition theorem of the Bessel functions[14] to the first two terms is applied, we obtain:

$$F(x) = (\pi/2^{1/2}) \sum \left[J_o(\pi n) . J_o(x \pi n) . J_o(1/4 x \pi) - 2^{1/2} J_o(q_n) J_1 (x \pi n) J_1 (1/4 x) \right]$$

Consider the first term in this expression, i.e.:

$$F_1 (x) = (\pi/2) \sum J_o(x \pi n) . J_o(\pi n)$$

Applying the product representation of Bessel functions[15]:

$$F_1 (x) = 1/2 \sum \int_0^{\pi} J_o \left[\pi n (1 + x^2 - 2x . \cos u)^{1/2} \right] . du$$

and the Schloemilch series[16]:

$$\sum J_o(nx) = -1/2 + 1/x$$

we can sum the infinite series before evaluating the integral. Further we use the definite integral [17]:

$$\int_0^{\pi} (1 - 2p.\cos u + p^2)^{-1/2} du = 2K(p)$$

where K(p) is the elliptic integral of the first kind. Hence we find:

$$F_1(x) = 1/2 \left[(-1/2)\pi + (2/\pi) K(x)\right] \tag{33}$$

Since the remaining term is a first-order correction, we are free to replace πn by q_n, neglecting again $\pi/4$, we get:

$$F_2(x) = \sum J_o(q_n).J_1(xq_n)$$

or, using the asymptotic value for $J_o(q_n)$ again:

$$F_2(x) = \sum (2/\pi) J_1(xq_n).q_n^{-1}/J_o(q_n)$$

This is a summable Dini series whose result is:

$$F_2(x) = -\pi^{-1}x$$

Substituting $F_1(x)$ and $F_2(x)$ in the original expression, we get:

$$F(x) = 2^{-1/2} J_o(x\pi/4).\left[-\pi 2^{-1} + (2/\pi)K(x)\right] + x.J_1(x\pi/4) \tag{34}$$

As a numerical check we calculate F(0) = .40361 and compare this with the value obtained by direct summation of the series, giving .38485. The error is less than 5%.

3.2.3 Virtual Mass Ratio

The final efficiency departs from the transfer efficiency calculated above by the fact that along with the fluid, a metallic cone has to be accelerated, which by itself does not contribute to the penetrating action of the jet. Moreover, the mass m in (4) is not to be taken as the actual rest mass of the cone-fluid system but must contain the virtual mass of the fluid created by the flow itself. We shall now derive a first-order expression for the ratio of virtual to actual mass of the fluid.

The vertical component of the integrated pressure forces acting on the side of the cone is:

$$f_v = 2\pi \int_0^{r_1} rp.\sin^2\theta_o dr = 2\pi\theta^2 \int_0^{r_1} rp\ dr$$

and from the expression for the pressure in terms of the velocity potential and the solution (29):

$$f_v = 8\pi\gamma\theta_o^2 r_1^4 \rho \frac{dV}{dt} \sum q_n^{-2}\left(\frac{q_n}{\theta_o} + 3/2\right)^{-1}$$

The mass force is:

$$f_m = m.\frac{dV}{dt}$$

whence the virtual mass ratio:

$$\frac{f_v + f_m}{f_m} = 1 + 12\Omega^2 r_1 g^{-1} \sum q_n^{-2}\left(\frac{q_n}{\theta_o} + 3/2\right)^{-1}$$

The infinite series may be summed in terms of the ψ function (logarithmic derivative of the gamma function) to give:

$$\frac{f_v + f_m}{f_m} = 1 + \Omega^2 r_1 g^{-1}\left[1 - 48(9\pi\theta_o)^{-1}\left(\psi(5/4 + 3\theta_o/2\pi) - \psi\right)(5/4)\right] \qquad (35)$$

Substituting (25) for the angular velocity, one sees that in the case of a 12° cone, the virtual mass is increased by more than 60%.

3.3 Second Order Approximation

The first order approximation was derived on the assumption that only the pressure force was influenced by the curvature of the free surface, but that the resulting flow proceeded as if the interface were plane. We shall now attempt to improve upon this approximation by partially taking account of the fact that the pressure condition (26) is to be applied to the actual shape of the meniscus rather than to its rest condition. We write the equation for the parabolic meniscus in polar co-ordinates as follows:

$$r/H_o = 1 - \alpha + \beta\,(\theta^2/\theta_o^2) \qquad (36)$$

where α and β are constants depending on the speed of rotation. In the following we shall utilize a non-dimensional parameter S which fully describes the motion, together with the cone apex angle θ_o:

$$S = \Omega^2 \theta_o H_o/(2g) = Fr/(8Ro^2) \tag{37}$$

where Fr is the Froude number and Ro the Rossby number referred to the characteristic length $\theta_o H_o$. From the geometrical considerations of paragraph 3.1 it follows that:

$$\alpha = S\theta_o/2, \quad \beta = S\theta_o \tag{38}$$

The procedure to be followed subsequently involves the substitution of (36) in (27), where we have adopted H_o as reference length in place of H_1, expanding the resulting trinomial to first order according to the binomial theorem and replacing A_n by the sum of the two coefficients representing the coefficients of the Dini series for x^2 and x^4 multiplied by unknown constants a and b respectively. Since the whole series must equal the pressure on the meniscus and therefore be proportional to x^2, we must adjust the constants a and b in such a way that any terms in x^4 must vanish and that the coefficient of x^2 correspond to that on the right hand side. Neglecting -1/2 again relative to q_n/θ_o, expanding (36) raised to the power q_n/θ_o to two terms and substituting in (27), equating this to the pressure (28), we obtain:

$$\sum (a_n + b_n) \left[1-(q_m/\theta_o)(\alpha - \beta x^2)\right] J_o(q_n x) = V\gamma\theta_o^2 H_o^2 x^2$$

where:

$$a_n = 4aq_n^{-2}/J_o(q_n), \quad b_n = 8bq_n^{-2}(1-8/q_n^2)/J_o(q_n)$$

are respectively the coefficients of the Dini series representing ax^2 and bx^4. Summing the resulting series, there results:

$$ax^2 - \frac{4a}{\theta_o}(\alpha - \beta x^2).F(x) + bx^4 = V\gamma\theta_o^2 H_o^2 x^2 \tag{39}$$

where F(x) is the function given in (34). Note that the term resulting from multiplication of the series for bx^4 with q_n has been omitted, in accordance with order-of-magnitude consideration. F(x) must now be expanded in terms of x^2 and a and b must be chosen such that the x^4 term disappears and the x^2 term balances against the right hand side of (39). From (34) we find:

$$F(x) = 2^{-1}2^{-1/2}(2 - \pi) + (1/2)x^2(1 + \pi/4)$$

whence the coefficients a and b:

$$a = \frac{V\gamma\theta_o^2 H_o^2}{1 + 2\beta(\theta_o)^{-1}2^{-1/2}(2 - \pi) - 2\alpha\theta_o^{-1}(1 + \pi/4)}$$

$$b = \frac{2\beta V\gamma\theta_o H_o^2(1 + 4^{-1}2^{1/2} + 4.2^{1/2}(\pi - 2))}{1 + 2\beta\theta_o^{-1}2^{-1/2}(2 - \pi) - 2\alpha\theta_o^{-1}(1 + \pi/4)}$$

Now, the quantity of greatest interest is the velocity of the head of the jet, i.e. $v_{ro} = v_r(\theta = 0) = \partial\phi/\partial r\ (\theta = 0)$. Returning to the series representation of the velocity potential:

$$v_{ro} = \sum\left[\frac{4(1 - \alpha)^{q_n\theta^{-1}-3/2}a}{\theta_o q_n J_o(q_n)} + \frac{8b}{\theta_o q_n J_o(q_n)}\left(1 - \frac{8}{q_n^2}\right)\right] \qquad (39a)$$

Note that in the second term the $1 - \alpha$ term has been omitted to keep orders of magnitude correct. The first term in this may be written, using the approximate value for q_n and the asymptotic expression for $J_o(q_n)$:

$$\sum (\pi/2).\exp.\left[(\pi n\theta^{-1} + (1/4)\pi\theta^{-1} - 3/2)\log(1 - \alpha)\right].J_o(\pi n).2^{1/2}$$

We expand $\log(1 - \alpha) = -\alpha$ and use the Schloemilch series[18] to the second order:

$$\sum J_o(n\pi).\exp.(nu) = -1/2 + (u^2 + \pi^2)^{-1/2} + u/12$$

The second term in (39a) was summed term by term and gave the value .77021.b. Taking all terms together and expanding a and b to first order in α and β we get finally:

$$v_{ro}/V = 2.2^{1/2}(-1 + \pi/2)S\ (1 - SU) \qquad (40)$$

where:

$$U = \frac{\pi^2}{24(-1 + \pi/2)} + (\pi/8) - (3/4)\theta_o - 1 - (\pi/4) - 2^{1/2}(\pi - 2) + \frac{.77021(1 + \pi/4)}{2^{1/2}(-1 + \pi/2)}$$

This is the second-order expression for the velocity amplifcation ratio, i.e. the factor by which the velocity of the cone is multiplied to obtain the velocity of the head of the jet.

It must be remembered that the whole treatment was carried out in a co-ordinate system travelling with the cone. To convert to a system at rest in the laboratory frame, one must add unity to (40). The largest possible value of this ratio is obtained for the case of critical rotational velocity (25). In this case $S = S_{max} = .31498/\theta_o$. In our experiments $\theta_o = \pi/15$. This yields in the laboratory frame:

$$(v_{ro}/V)_{max} = 6.12958$$

It is interesting to note that in first order of S_{max} v_{ro}/V becomes inversely proportional to θ_o this is in agreement with the findings of the classical theory of shaped charges [1].

3.4 Shape of Jet Profile for Small Times

From (29) it is possible to obtain the shape of the jet by simply integrating these equations with respect to time. It must be remembered that in this treatment the convection terms in Euler's equation were neglected; all solutions apply therefore only to small times. Hence, it is not necessary to proceed to the second order in calculating the jet profile, as the first order will yield enough information for the case of low distortion of the free surface.

Figure 9 shows a number of profiles calculated for progressively larger values of time. A distinctive feature of these curves is the rapid negative motion of the fluid near the cone wall. This is due to the logarithmic infinity of K(x) in (34) as x approaches one. In the experiments some breakup of the fluid is observed near this region, probably due to cavitation caused by the large negative pressures generated. In Figure 9 are also shown some experimental points taken from photographs of the developing jet. The agreement appears to be satisfactory in view of the assumptions made and the difficulty in maintaining good experimental conditions. Poorest agreement is found at earliest times, probably due to the fact that the initial free surface was not plane, as assumed in the first-order theory, but distorted by capillary action near the cone wall.

3.5 Stream Lines

The stream lines of the first-order solution can be obtained from the definition of the stream function ψ:

$$v_r = r^{-2}.\theta^{-1}\,\partial\psi/\partial\theta$$

$$v_\theta = -(r\theta)^{-1}\,\partial\psi/\partial r$$

hence from (29):

$$\psi = \sum A_n H_1 \theta (1 - \theta_o/2q_n).(r/H_1)^{(q_n/\theta_o)\ +\ 1/2}.J_1(q_n\vartheta/\theta_o) \qquad (41)$$

where A_n are the coefficients of the Dini series given before. The stream lines are shown plotted in Figure 10 for the case of a cone of 24° included apex angle (θ_o = 12°). The large negative velocities near the cone wall are again apparent in this figure, as well as the cumulation of stream lines near the axis of the cone where the jet is formed. It must be noted that the stream function (41) applies to a frame of reference fixed in the moving cone; for a frame stationary in the laboratory, the term:

$$\psi_o = -Vr^2\theta^2/2$$

must be added to (41).

4.0 EXPERIMENTS

4.1 General Considerations

The experimental rig consists essentially of a condenser bank discharging into a conical single-turn coil carrying the rotating cone. The similarity with a plasma pinch (theta pinch) experiment is obvious; however the design criteria are somewhat different. As in the plasma pinch, the time constant of the discharge must be kept small to ensure that the magnetic field of the coil does not penetrate through the wall of the cone. This is usually achieved by keeping the circuit inductance L_o as small as possible, a requirement which also guarantees that the inductance coefficient Q (19) remains small. On the other hand it is seen from (4) that for greater transfer efficiency the variable inductance L_1 must be made large. Since most of the circuit inductance is located in the condenser bank and the external conductors, a transformer designed to match L_1 into the primary circuit could be used to optimize the efficiency. Unfortunately, the high frequency of the discharge transient precludes the use of iron transformer cores; the use of ferrite as core material is the next best choice, though even in this case the transformer develops a considerable leakage inductance. The compromise finally adopted comprised a ferrite-cored step-down transformer of ratio 40:1.

4.2 Transformer and Coil

The schematic of the transformer is shown in Figure 11. The ferrite core is eveloped in a thin layer of mylar sheet insulation which carries the 40-turn primary wound with square-section magnet wire. A further layer of insulation separates this from the secondary which is a 1/8 inch thick split copper tube, which in turn is encased in a 1/2 inch thick cylinder of steel to prevent the coil from spreading under the action of the magnetic pressure. The conical pinch coil is silver-soldered to the gap in the secondary and is held firmly to the transformer by means of a 1/2 inch retainer plate bolted to two jaws welded to the steel cylinder. The coil itself is a split brass block of square section, carrying a conical hole into which fits the rotating cone. The coil is fitted with an air bearing supplied through a nozzle, while a second nozzle supplies air tangentially to the cone to provide the torque necessary to set the cone into rotating motion. The transformer is held between two plexiglass rings and three steel bolts. Figure 12 shows a photograph of the transformer-coil assembly.

The variable inductance L_1 was measured by mounting the cone, made of aluminum on a traversing rig, the coil being clamped firmly to the base of the rig and the displacement of the cone being measured with a dial gauge. The inductance was measured on a Hewlett-Packard R-X meter (Schering Bridge) using a suitable frequency of the order of megahertz. The readings had to be modified to take account of the lower working frequencies in the discharge circuit, owing to the greater penetration of the magnetic field. (Fig. 3).

4.3 Linear Velocity Measurements

The transformer-and-coil assembly was installed in the discharge circuit and the condenser bank charged to a voltage varying between 1200 and 7100 V. The air cushion on which the cone floats is, as a rule sufficient insulation to prevent the cone from shorting out the coil. For greater safety at high levels of condenser voltage the cone external surface was anodized.

The "muzzle velocity" with which the cone leaves the coil on discharge was measured optically by projecting a collimated beam of light horizontally over the cone, through a 45° glass splitter plate and back again as a parallel beam about 2 inches above the first. The light from this beam, together with a portion of the first beam separated from it by a half-silvered mirror, enters a photodiode the output of which actuates an electronic interval counter. The discharge current is simultaneously monitored with the aid of a Rogowski coil around one of the conductors, and an oscilloscope. The damped oscillatory signal obtained is analyzed to obtain the frequency and hence the circuit inductance L_o, while the damping yields the total loss resistance R. As the transfer efficiency was found to be quite small, the approximate expression (24) was used for comparison with experimental values. Results are shown in Figure 6. The apparent break in the experimental curve around 4 kV is caused by the fact that for operation with higher voltages, the pressure supplying the air bearing had to be increased to avoid flashover between coil and cone, the resulting increase in the air gap giving a small change in the readings.

4.4 Photographic Experiments

To compare the hydrodynamic calculations with experiment, it was necessary to take high-speed photographs of the development of the jet. The setup used is shown in the block diagram Figure 13. The output from the Rogowski coil is fed into an amplifier whose output actuates the start circuit of the interval counter. A second output signal is retarded by a delay generator which supplies a stop signal to the counter. A signal is taken from one of the decade circuits of the counter, amplified and fed into the flash unit which supplies the high voltage needed to trigger a xenon flash tube[19]. Each time the decade cycles through its period, it emits a pulse which normally goes to switch on a digit light on the counter. This pulse is thus made to trigger the flash circuit. Up to 2500 Hz of repetition frequency is attainable in this way. A Tektronix time mark generator is used to calibrate the delay circuit.

The burst of flashes (duration 1/2 microsecond) illuminates the object while the film of a NRC-Dudgeon drum camera[20] is being exposed. This camera has a hollow drum carrying the film on the inside surface and mounted on air bearings and driven by an air turbine. Simultaneously, the rotational speed of the cone is measured by means

of a marker painted on the edge of the cone whose motion is detected by a light and photo-transistor. The period between successive passages of the marker past the photo pickup is measured on another interval counter. The rotational speed of the drum camera is monitored on an oscilloscope.

For better photographic contrast the cone was partially filled with milk, instead of water. Typical results are shown in Figure 14, representing shots at different condenser voltages and cone rotational speeds. The voltage seems to have only minor effect on the shape of the jet, except at high voltage when the head of the jet seems to develop a plume of spray. This is seen more clearly on Figure 15 which shows a single flash picture taken with a still camera. This plume appears to be caused by the drag in the stagnation point boundary layer of the surrounding air. The resulting loss of fluid and hence of apparent forward speed of the jet head causes some difficulty in interpreting the results, as will be seen in the following. In addition, the high voltage shots also show the development of a thin precursor jet. It is thought that this jet is produced by the elastic contraction of the cone under the magnetic driving field. In the appendix is given a mathematical treatment, supported by experiments, of the magnetic field inside a conical coil. It is seen that the field rises steeply from the upper edge of the cone to the apex, a course which might account for the small thickness of the precursor jet.

It has been assumed in the mathematical analysis that the effect of rotation on the motion of the fluid (as opposed to the development of the meniscus) can be neglected. This is certainly true for the early phases of the motion and at high driving voltages. At low voltage and at later times, however, Figure 16 shows definite indication of rotational effects. These are magnified by the fact that, as can be seen from the stream lines Figure 10, the fluid starting near the wall of the cone is forced toward the centre to form the jet. Due to conservation of rotary momentum, the angular speed of the fluid composing the jet surface may attain considerable magnitudes. This is shown in Figure 16 where the jet edge is seen to be subject to typical centrifugal instability, resulting in the ejection of droplets[21].

In Figure 17 is seen a series of exposures depicting the penetration of a paper target by a jet produced by a 6 kV discharge. By connecting the jet head position by a straight line, it can be seen that penetration occurs instantaneously. The precursor jet is eliminated in the process and the plume is somewhat reduced.

4.5 Velocity Amplification: Comparison

From a technical point of view, the most important quantity is the factor by which the head-of-the-jet velocity is amplified relative to that of the cone, i.e. the velocity amplification. An analytical expression of this quantity is given in (40). Comparison with experimental findings was made simply by measuring the respective slopes of the cone and jet exposures, Figure 14. Absolute values of velocity are easily obtained bearing in mind the fact that the flashing rate and hence the time between exposures is tightly synchronized with the cycling rate of the counter decade. The scale of the pictures is obtained by exposing a measuring scale in place of the jet. Values of velocity thus obtained are found to agree closely with those measured photoelectrically in 4.3, taking into account the total mass of cone plus fluid, including the virtual mass. Comparison between theoretical and experimentally determined velocity amplification vs rotational speed of the cone is made in Figure 18. It will be seen that the experimental points

agree with the theoretical curve for low values of angular velocity but begin to diverge for higher values, and that the agreement is maintained for higher angular speeds for results obtained with lower driving voltages. This is explained in terms of lateral loss of fluid of the jet head as a result of the dispersal of fluid in the plume. Note that the curves are displaced vertically so that they pass through a point somewhat larger than unity as required by theory. This is due to the fact that even at zero rotational speed the meniscus is somewhat concave, owing to the presence of interfacial tension between the fluid and the cone material.

5.0 CONCLUSIONS

It is shown that the mechanics of the explosively driven Monroe jet (shaped charge effect) can be simulated by means of a fluid in a rotating and vertically accelerated cone. The theory of the electromagnetic propulsion of the cone by means of a condenser discharge can be developed in terms of the WKB approximation. The hydrodynamic theory, assuming an ideal, inviscid and incompressible fluid is carried out in a two-step procedure, where the velocity amplification results from a second order approximation. Good agreement is found with theory for such conditions where the velocity of the jet head is comparatively low; at higher velocities the jet tends to be dispersed by frictional interaction with the surrounding air, making the apparent jet velocity somewhat lower than predicted.

From the point of view of technological application, the coupling between condenser energy and cone that could be attained in the present experiments was rather poor, resulting in a maximum apparent jet velocity of 230 ft/sec (extrapolating for plume loss, this figure may be increased by a factor of 3). It is proposed to redesign the electromagnetic propulsion device in order to improve both the "circuit Mach number" M and the inductance coefficient Q. This should result in a much greater jet velocity attainable. An intrinsic drawback of this device is the necessity to operate it vertically.

6.0 ACKNOWLEDGEMENTS

We are greatly indebted to Mr. A.J. Bachmeier for suggesting this problem and to Mr. M.J. Woodward, Mr. B. Mongeau and Mr. S.Y. Ho for some preliminary experimental work. Our thanks are also due to Dr. I.R.G. Lowe for the design of the air bearing and Dr. J. Lau for help with computational work. The technical help of Mr. G. Boult, Mr. W.C. Michie and Mr. J. Margerum is also greatly appreciated.

7.0 REFERENCES

1. Birkhoff, MacDougall, Pugh, Taylor — J. Appl. Phys. Vol. 19, 1948, p. 563.

2. Clark, J.C. — J. Appl. Phys. Vol. 20, 1949, p. 363.

3.	Pugh Eichelberger Rostoker	J. Appl. Phys. Vol. 23, No. 5, 1952, p. 532.
4.	Eichelberger, R.J. Pugh, E.M.	J. Appl. Phys. Vol. 23, No. 5, 1952, p. 537.
5.	Bless, S.J.	J. Appl. Phys. Vol. 43, No. 4, 1972, p. 1580.
6.	Millsaps, K. Pohlhausen, K.	Holloman Air Development Center, Operations Research Office. Tech. Memo. No. 3, 1950.
7.	Mostov, P.M. Neuringer, J.L. Rigney, D.S.	Phys. Fluids, Vol. 4, No. 9, 1961, p. 1097.
8.	Morse, P.M. Feshbach, H.	Methods of Theoretical Physics. McGraw-Hill, 1953, p. 1092.
9.	Savic, P.	Electrical Explosions. (To be published).
10.		Handbook of Mathematical Functions. Nat. Bur. Standards (U.S.), Appl. Math. Ser. No. 55, pp. 505-507.
11.	Gradshteyn Ryzhik, I.M.	Tables of Integrals, Series and Products. Academic Press., 1965, p. 479.
12.		See (10), formula 7.4.2., p. 302.
13.	Penney, W.G. Thornhill, C.K.	Phil. Trans. Roy. Soc., Ser. A, No. 882, Vol. 244, 1952, p. 285.
14.		Ref. 11, formula 8.531(1), p. 979.
15.	Magnus, W. Oberhettinger, F. Soni, R.P.	Formulas and Theorems for the Special Functions of Mathematical Physics. Springer-Verlag N.Y., 1966, p. 95.
16.		See (11), formula 8.521.1., p. 976.
17.		ibid., formula 3.674.1., p. 387.
18.		See (15), p. 131.
19.	Savic, P. Mongeau, B.	A Rapid Flash Burst Circuit for High-Speed Photography. (To be published).

20. Dudgeon, E.H. Proc. 5th Int. Congress High-Speed Photography, 1962, p. 303.

21. Drummond, A.M. On Atomization and Linearized Free-Surface Instability on Rotating Bodies.
NAE Aero Rep. LR-561, June 1972.

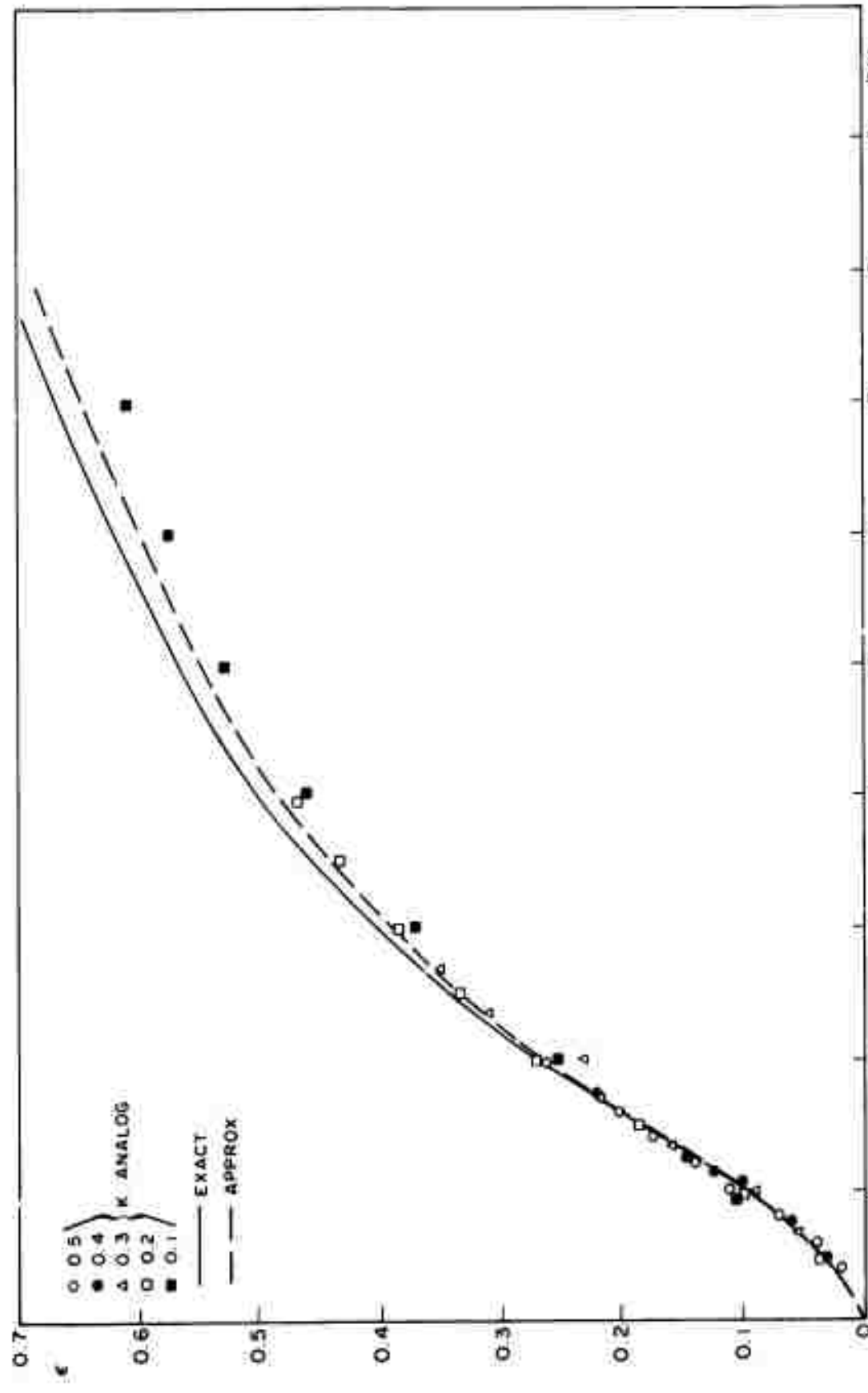

FIG.1: TRANSFER EFFICIENCY vs P/K. COMPARISON OF EXACT, APPROXIMATE AND ANALOG SOLUTIONS

Preceding page blank

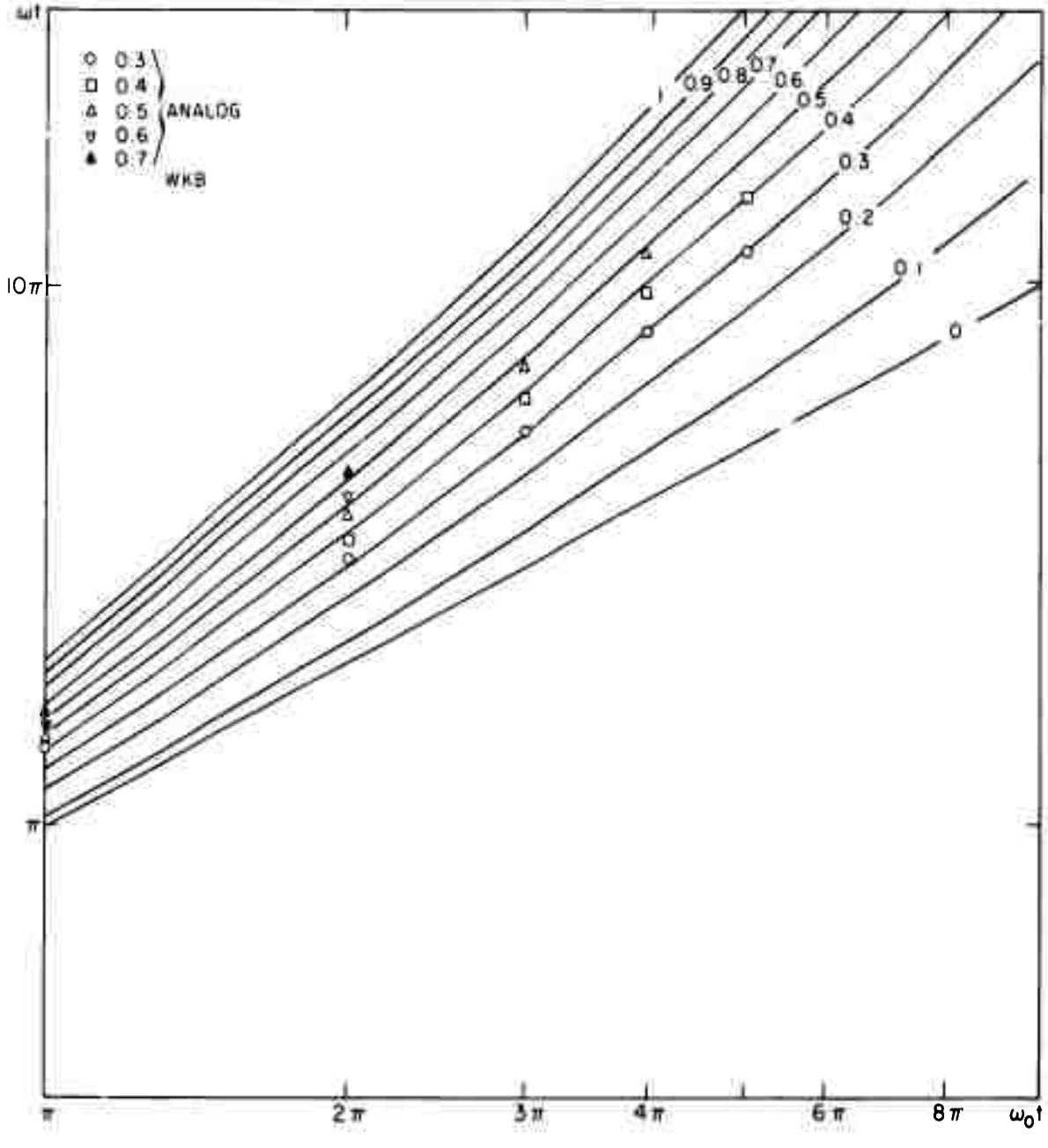

FIG. 2: POSITION OF ZEROS OF DISCHARGE CURRENT. COMPARISON OF ANALOG AND WKB SOLUTIONS

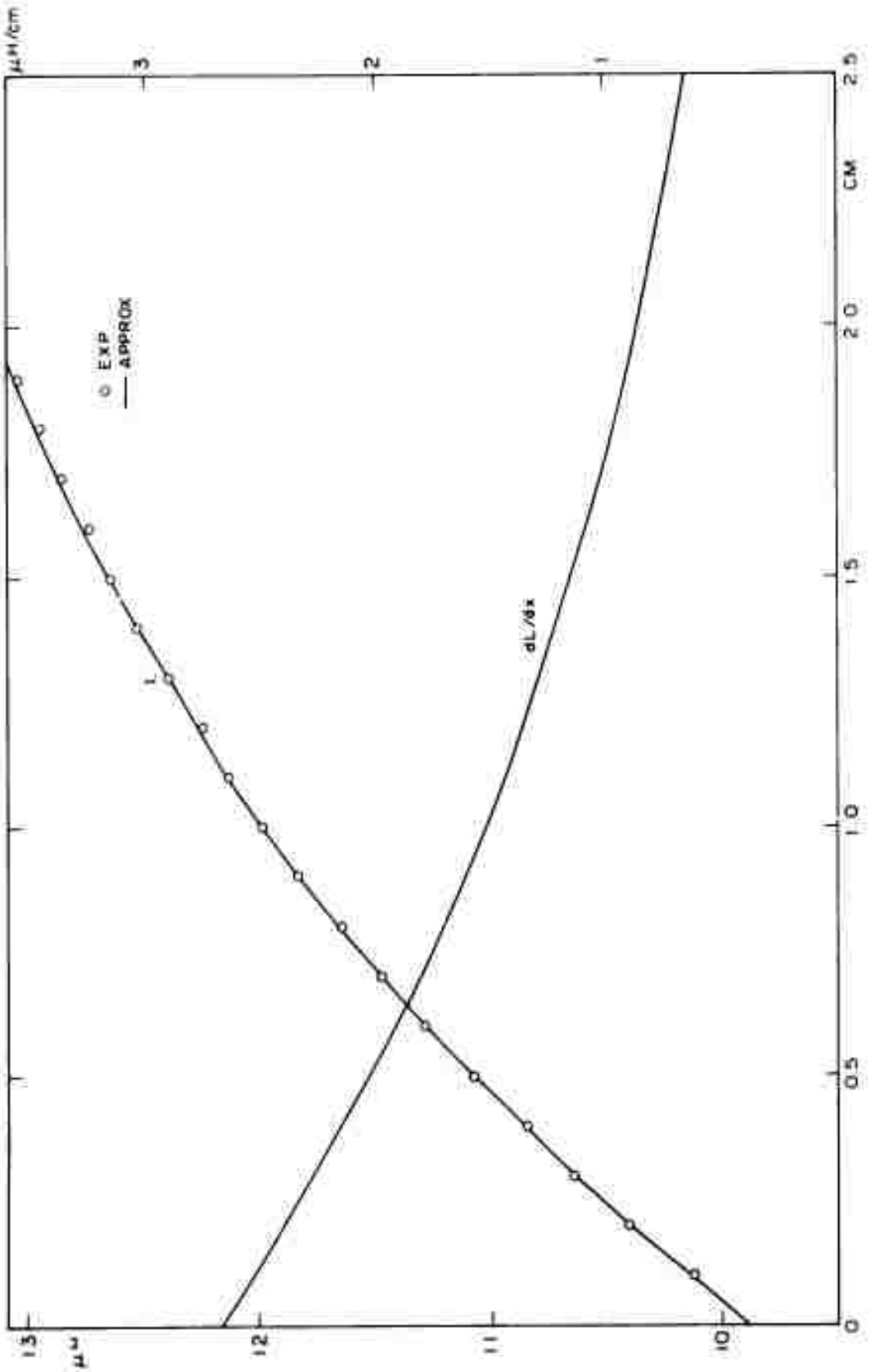

FIG.3: CURVE FIT OF EXPERIMENTAL INDUCTANCE-DISPLACEMENT RESULTS WITH EXPONENTIAL FUNCTION

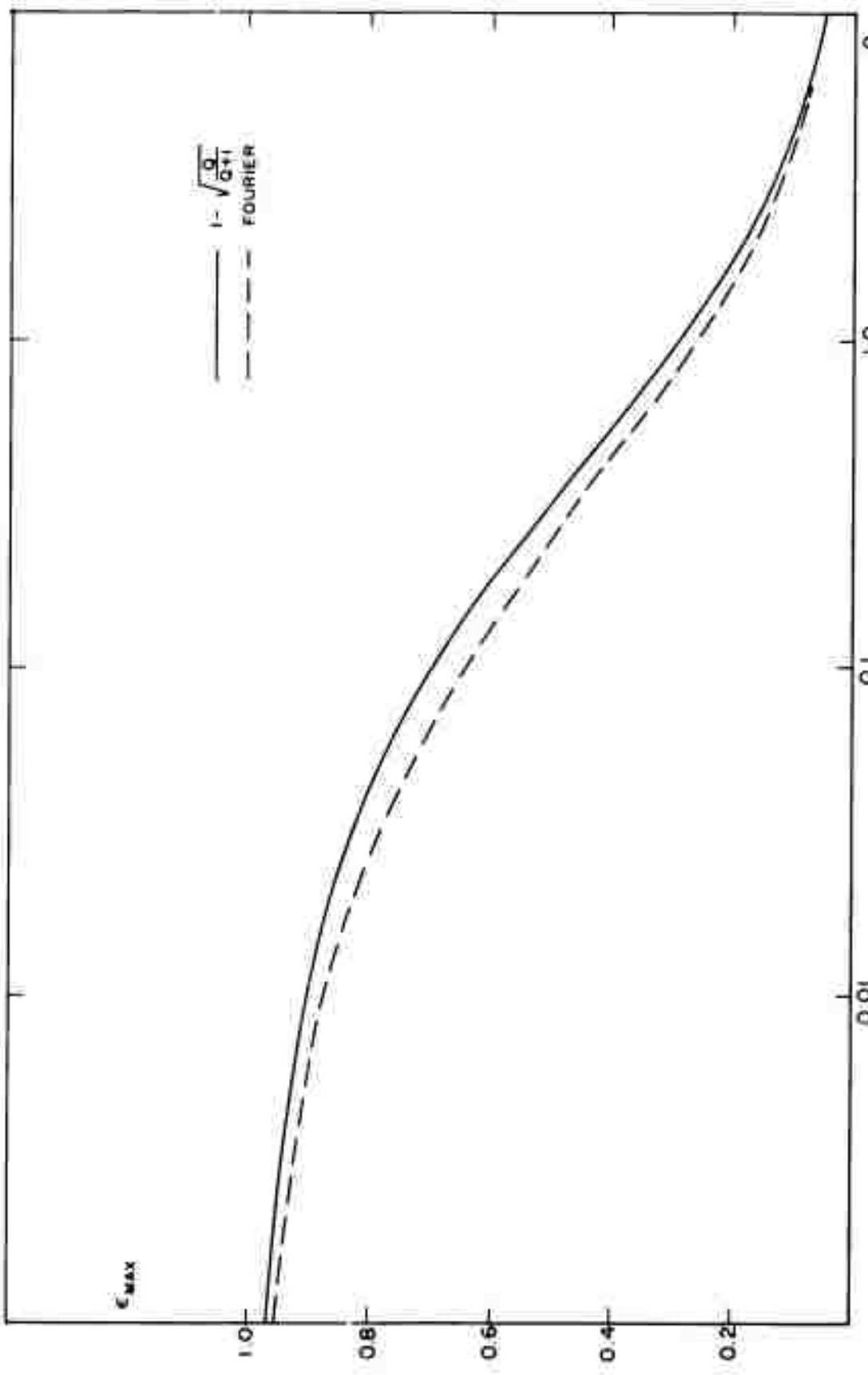

FIG.4: MAXIMUM TRANSFER EFFICIENCY vs Q COMPARISON OF DIRECT SOLUTION AND THREE-TERM FOURIER SERIES

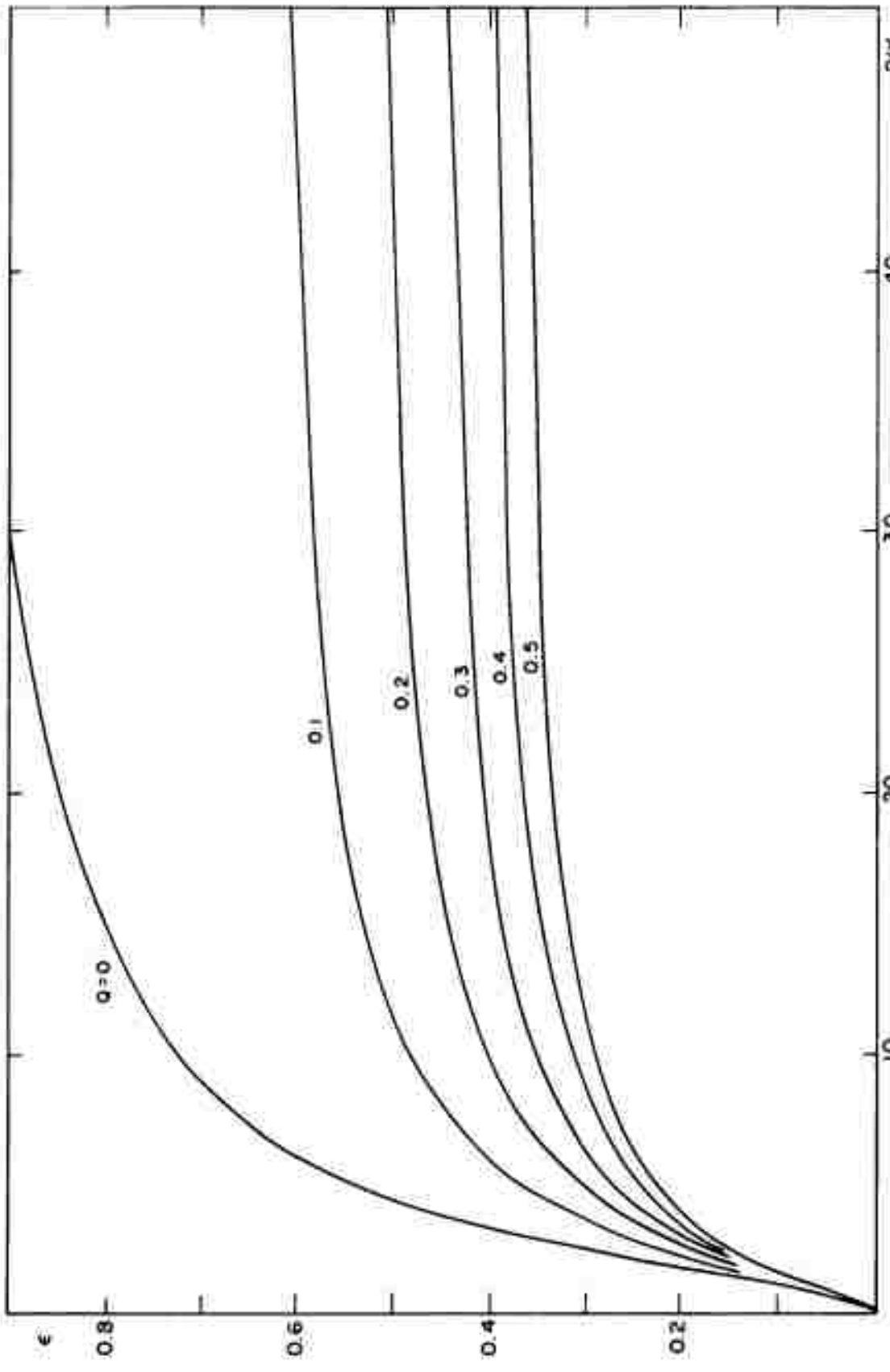

FIG.5: TRANSFER EFFICIENCY vs P/K FOR DIFFERENT VALUES OF Q

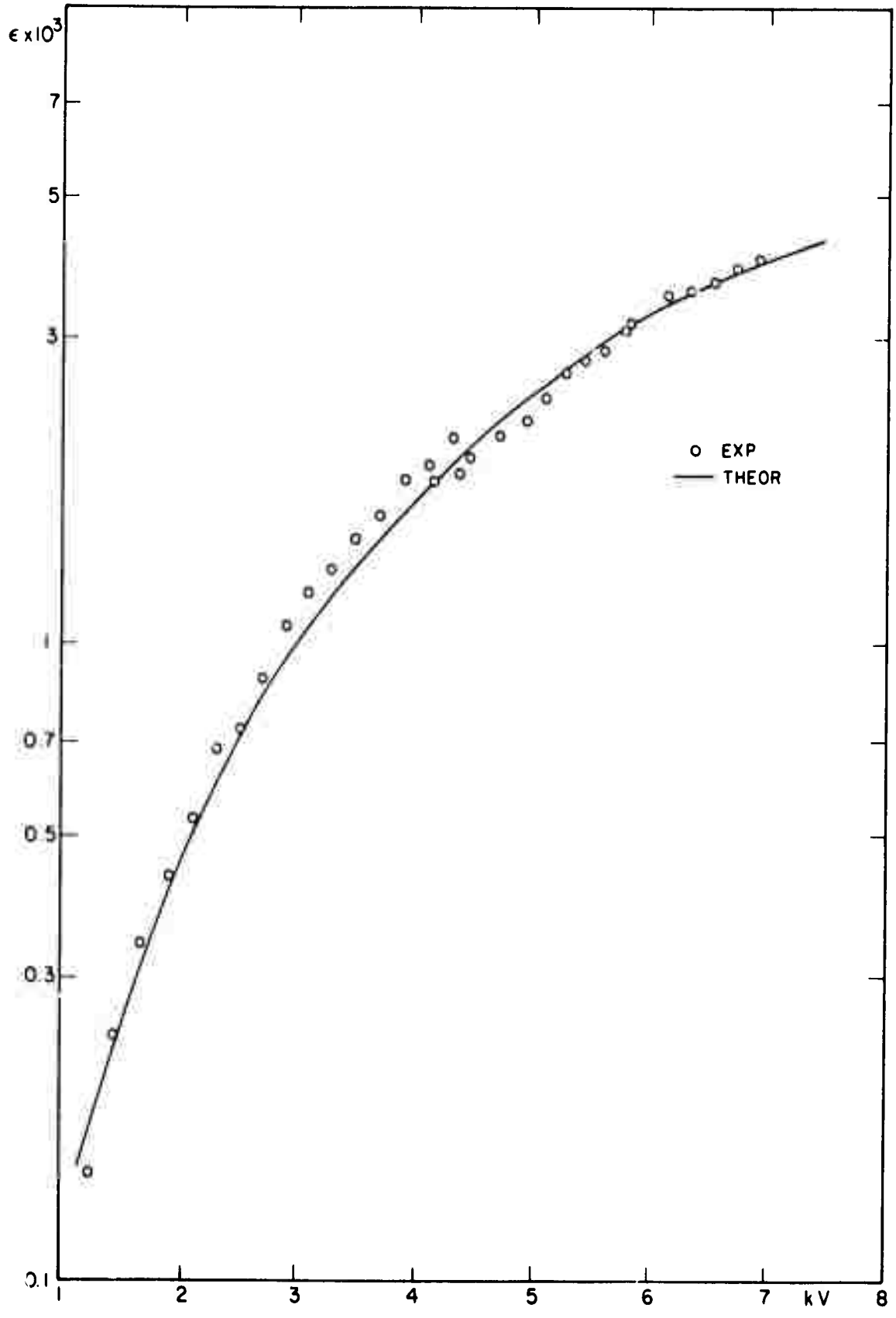

FIG.6: TRANSFER EFFICIENCY vs CONDENSER VOLTAGE. COMPARISON WITH PHOTOELECTRIC SPEED MEASUREMENTS

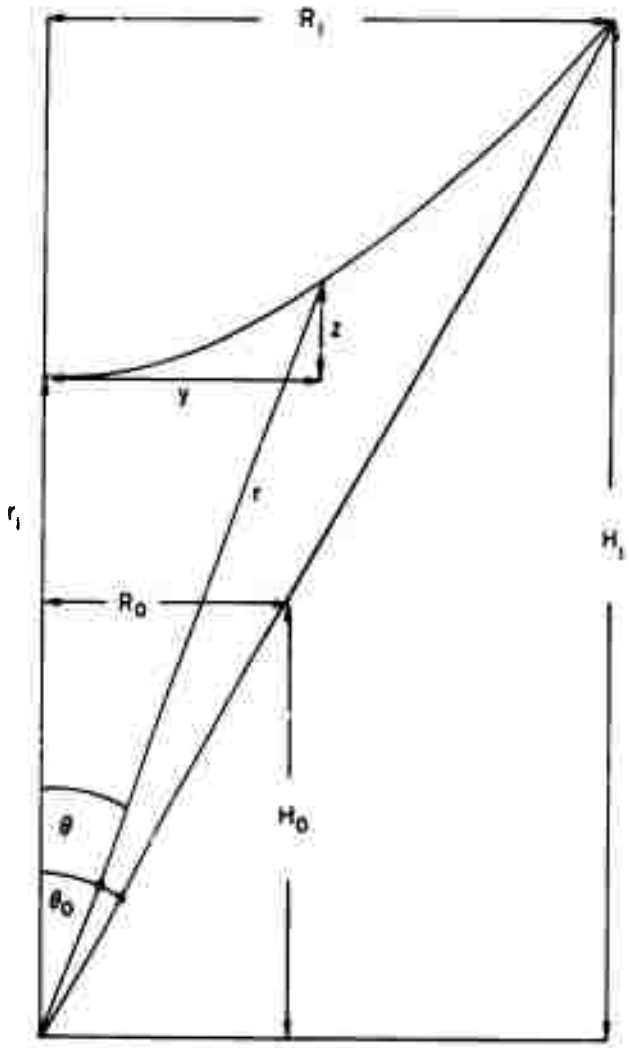

FIG. 7: CO-ORDINATE SYSTEM

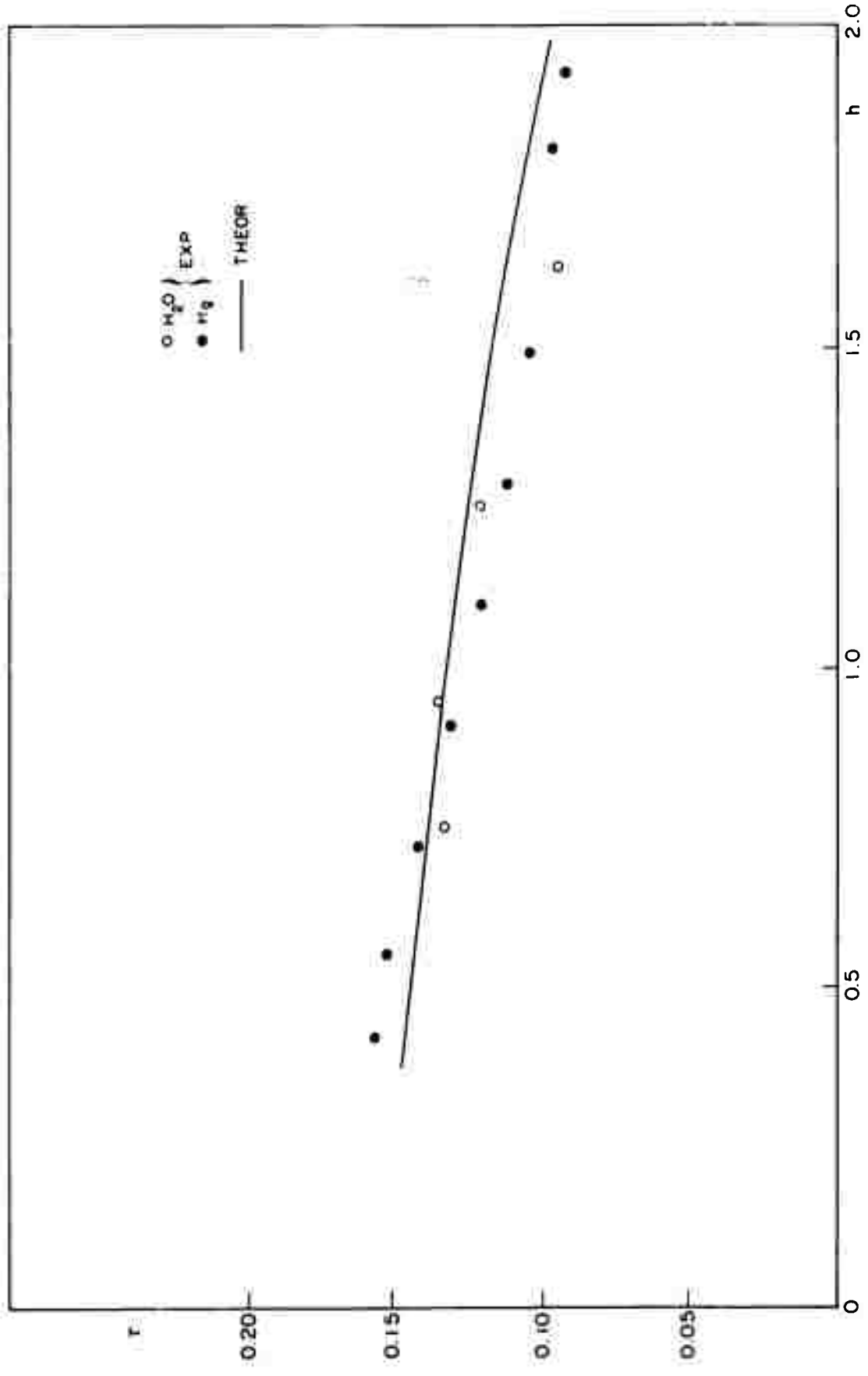

FIG.8: CRITICAL ROTATIONAL PERIOD OF POOL OF LIQUID IN CONE vs INITIAL FILLING DEPTH. COMPARISON WITH EXPERIMENTS

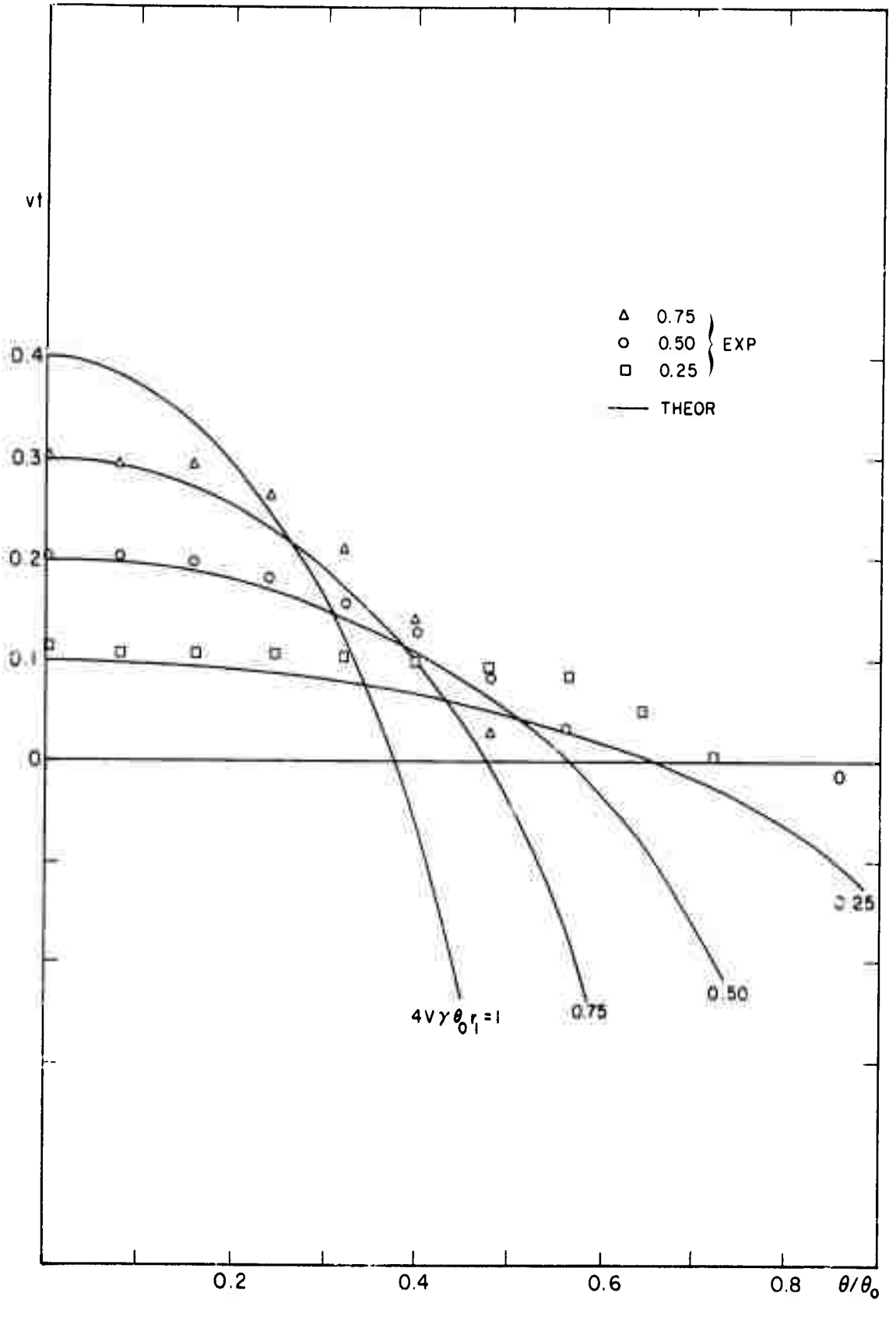

FIG.9: SHAPE OF JET FOR EARLY TIMES. COMPARISON WITH PHOTOGRAPHS

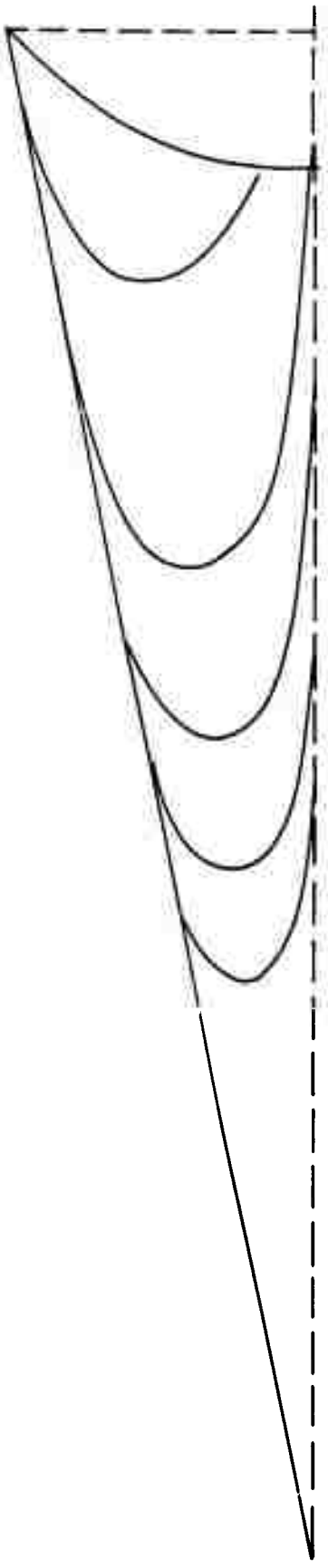

FIG. 10: STREAMLINE IN HALF-CONE FOR FRAME AT REST IN CONE

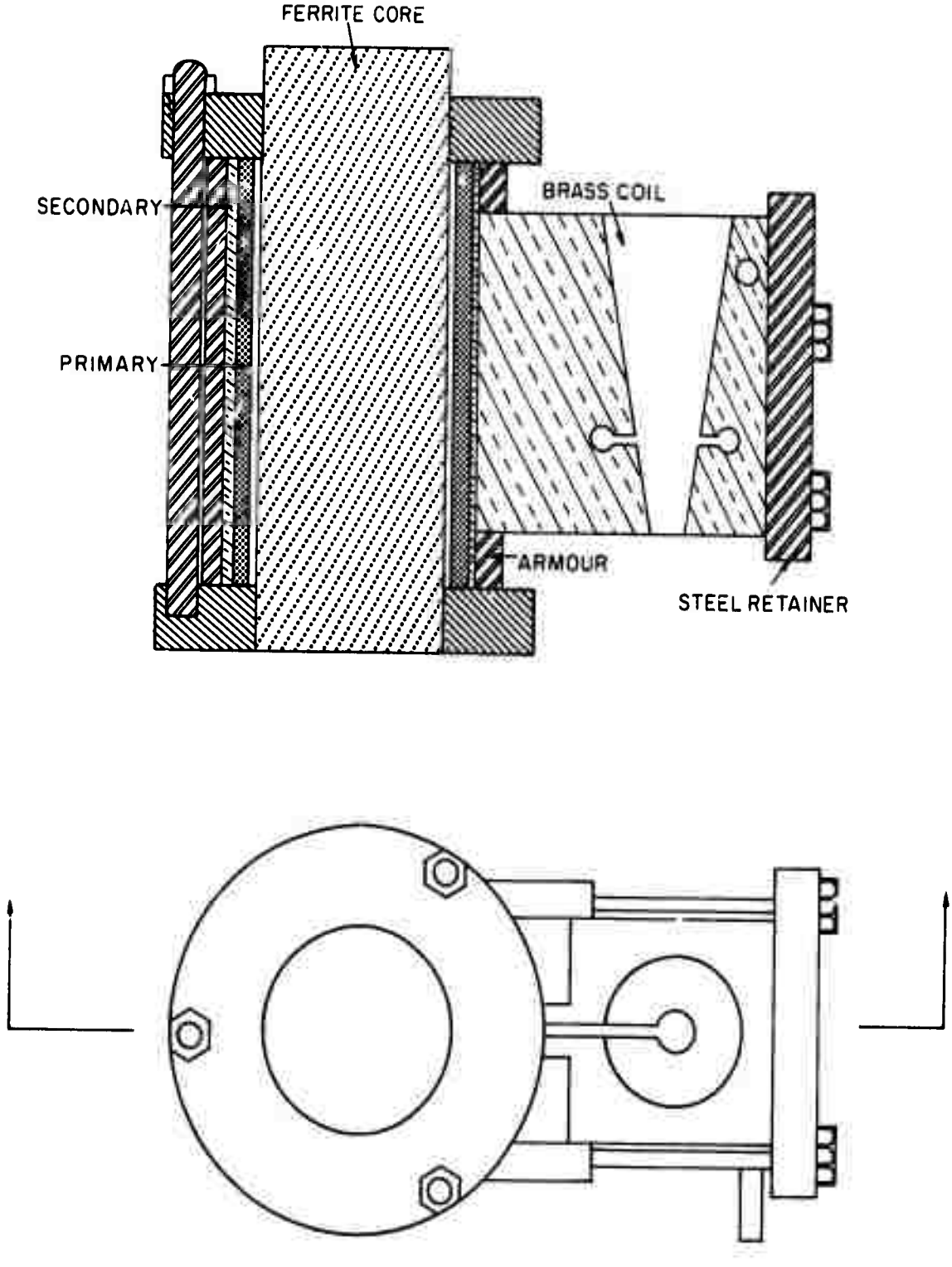

FIG. II: SCHEMATIC OF TRANSFORMER AND COIL

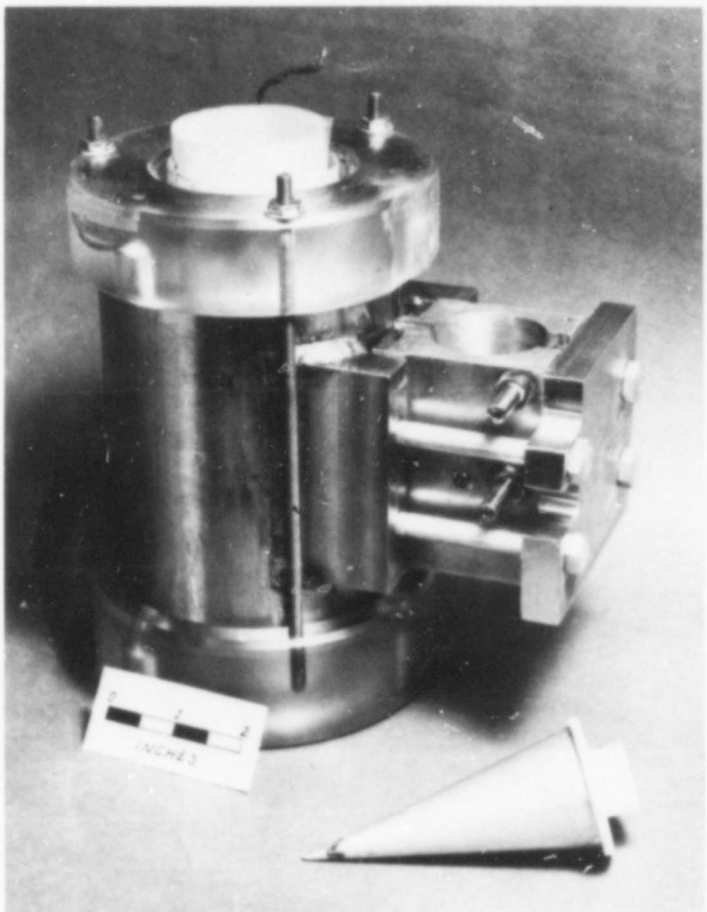

FIG. 12: PHOTOGRAPH OF TRANSFORMER AND COIL

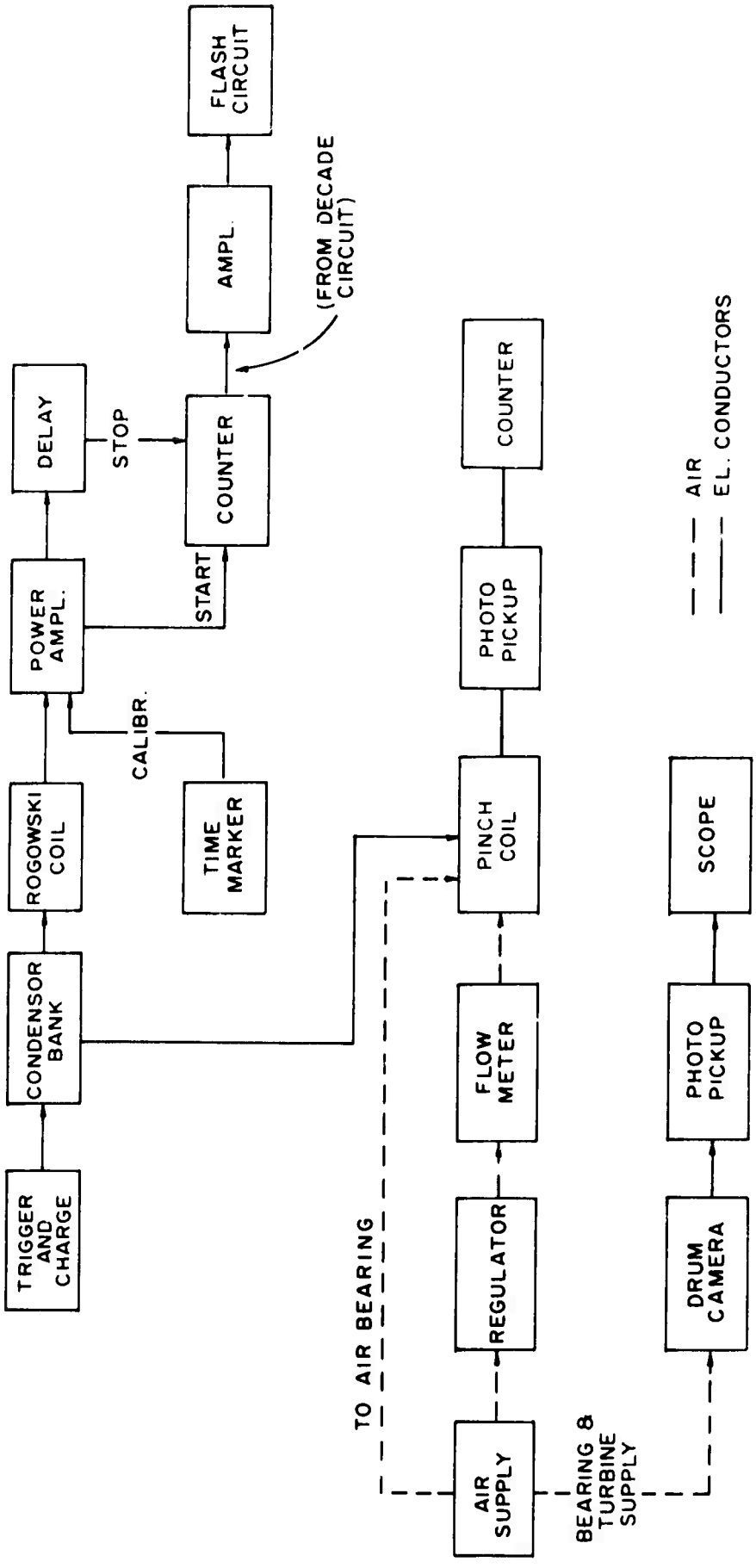

FIG. 13: BLOCK DIAGRAM OF PHOTOGRAPHIC EXPERIMENT

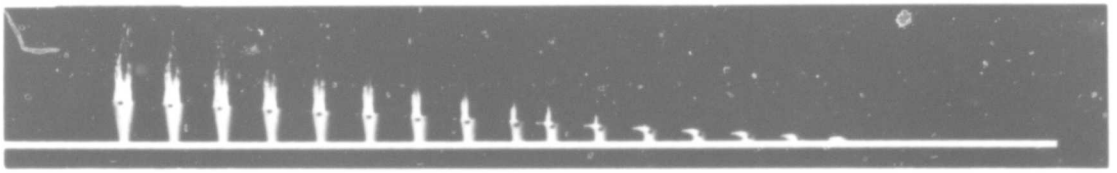

(a) V_0 = 2kV, ROT. SPEED = 7.35 rps

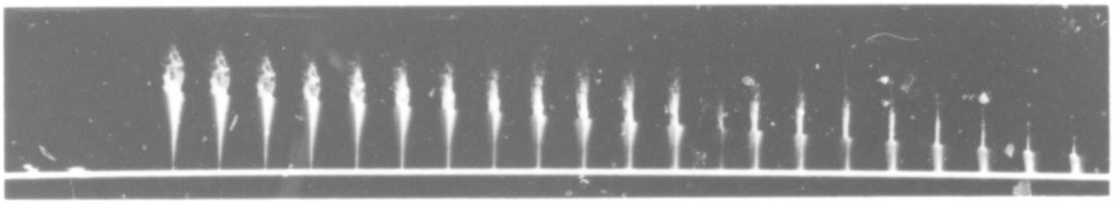

(b) V_0 = 3kV, ROT. SPEED = 8.69 rps

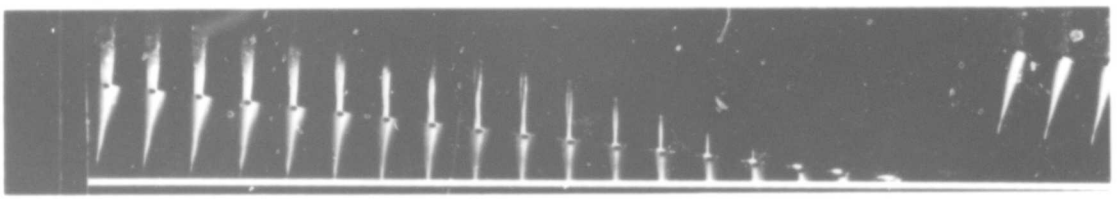

(c) V_0 = 4kV, ROT. SPEED = 7.46rps

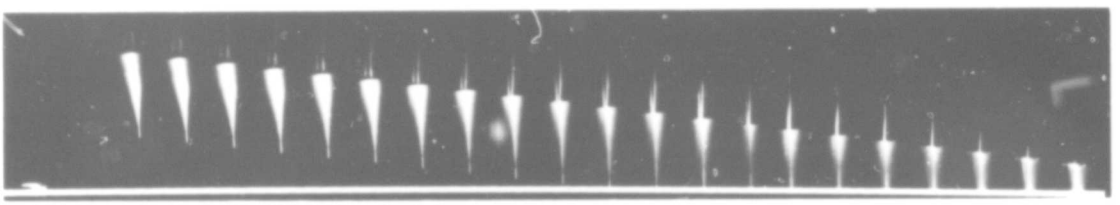

(d) V_0 = 4kV, ROT. SPEED = 5.26 rps

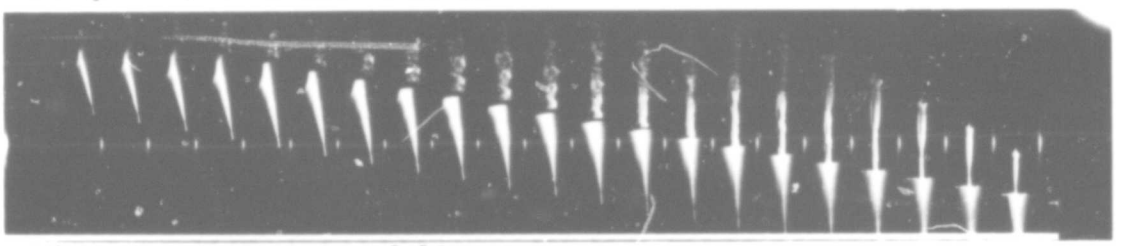

(e) V_0 = 5kV, ROT. SPEED = 8.26 rps

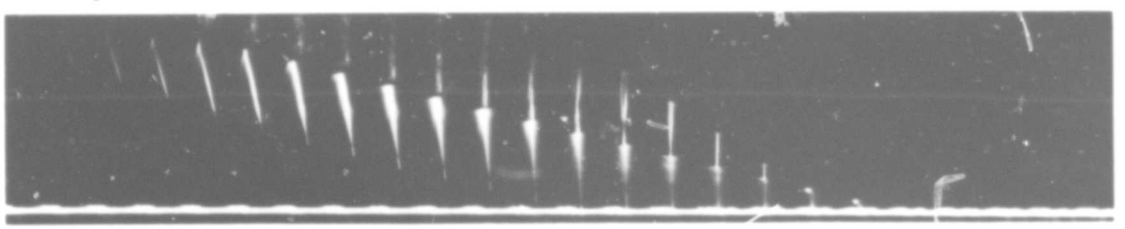

(f) V_0 = 6k V, ROT. SPEED = 8.20 rps

FIG.14: PHOTOGRAPHS OF DEVELOPING JET IN CONE

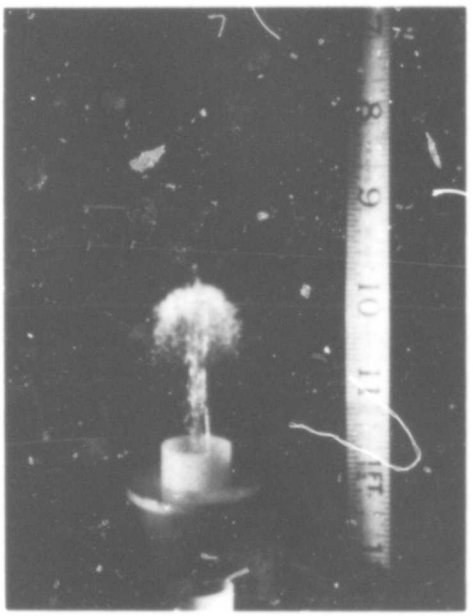

FIG. 15: STILL PHOTOGRAPH OF JET WITH PLUME
V_0 = 6 kV ROT SPEED, 6.70 r p s

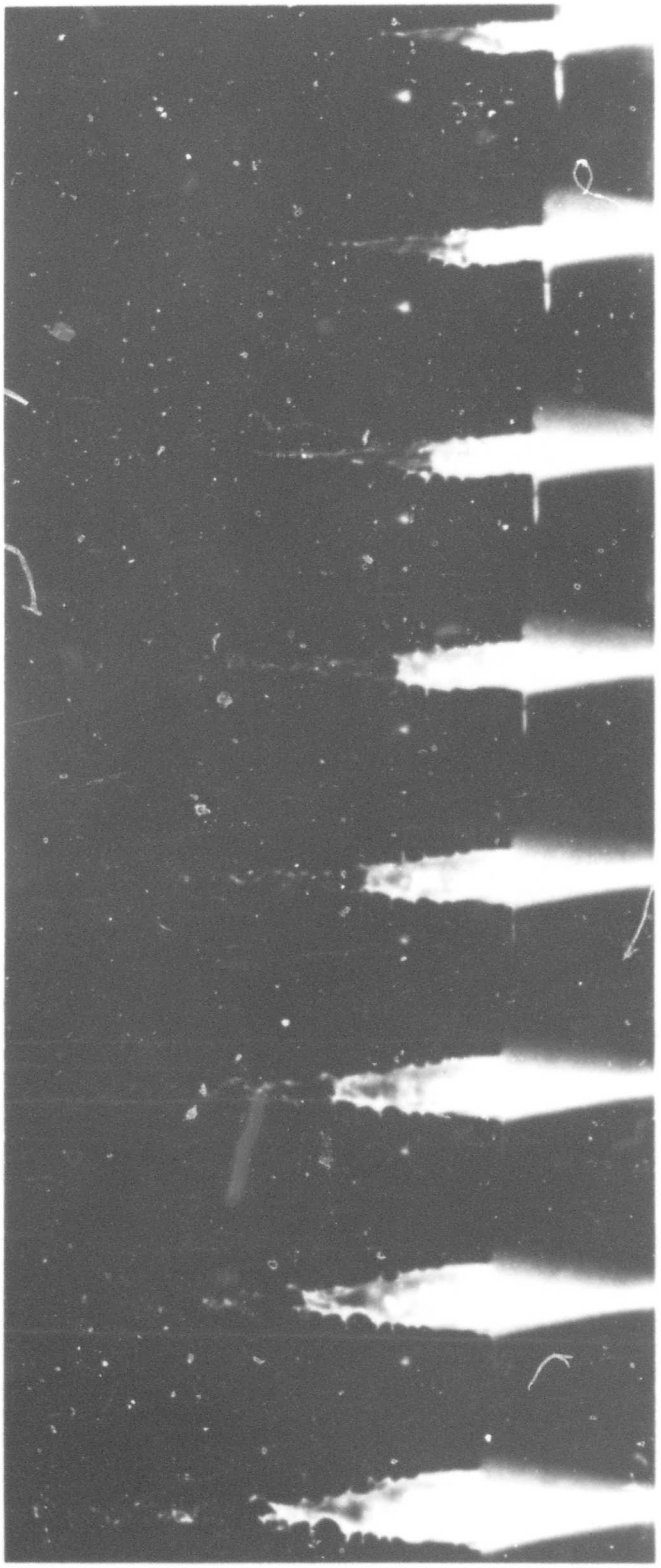

FIG. 16: DEVELOPMENT OF JET AT LOW VOLTAGE SHOWING ROTATIONAL INSTABILITY
V_o = 2 kV

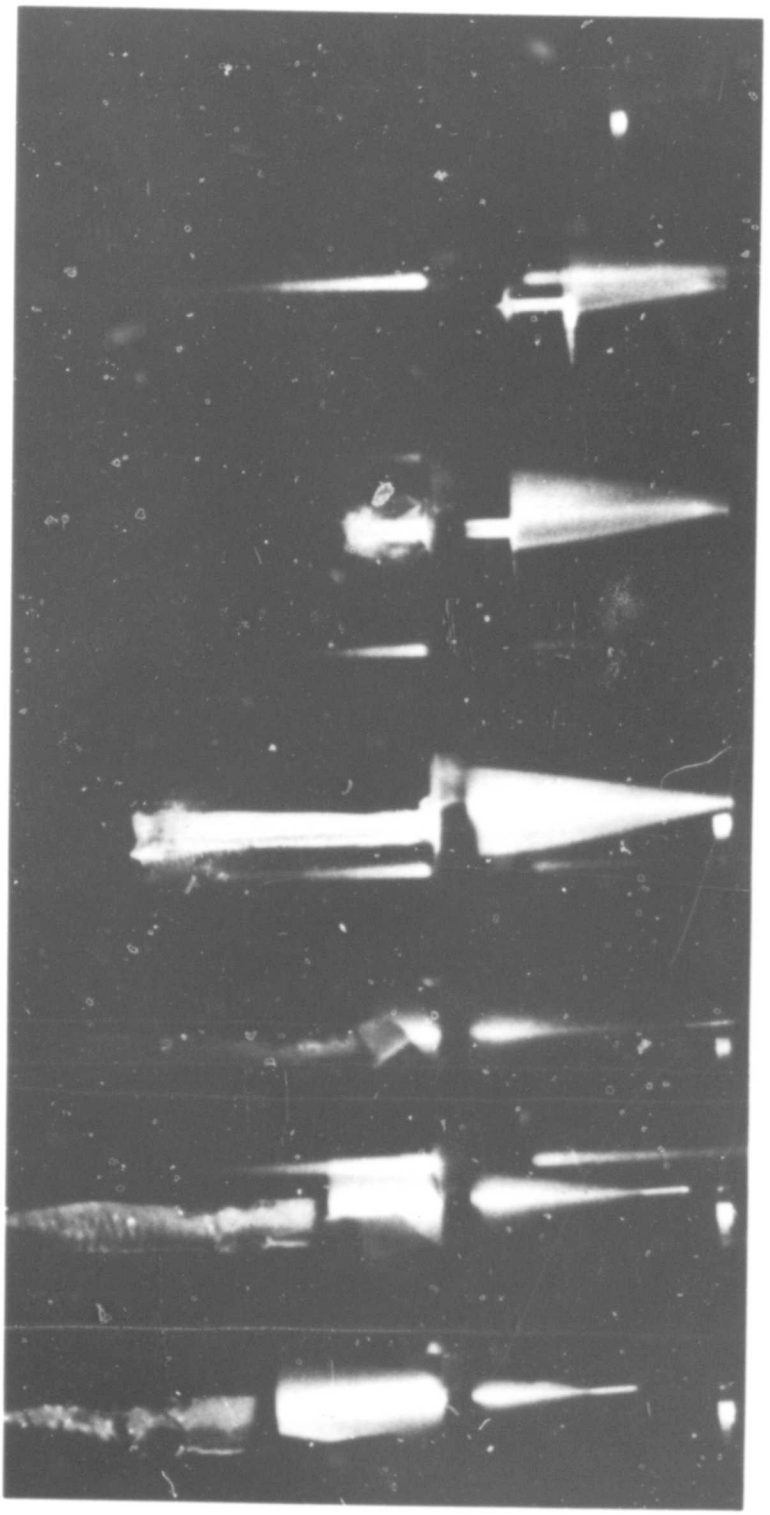

FIG.17 : PHOTOGRAPH SHOWING PENETRATION OF PAPER TARGET BY JET
V_0 = 6 k V

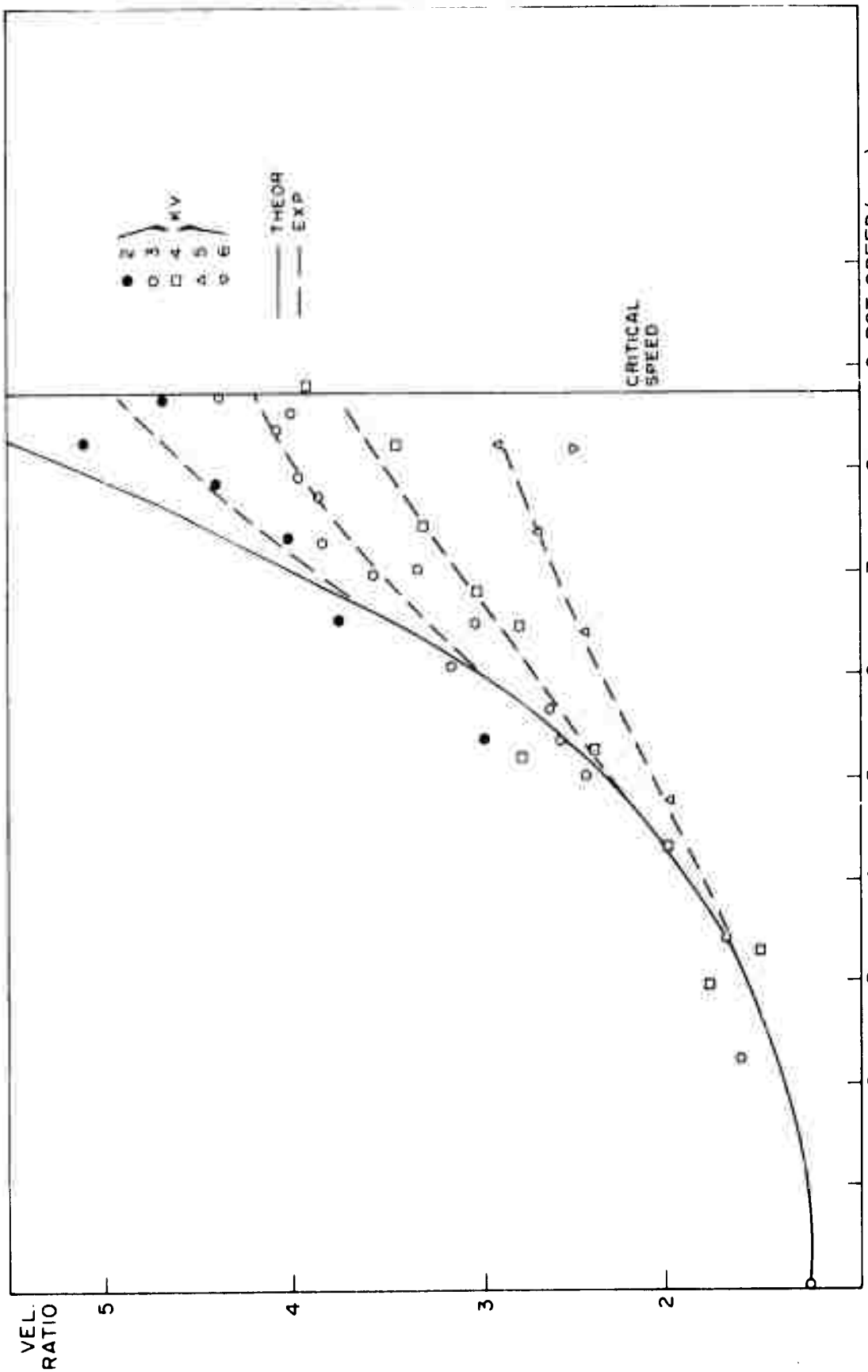

FIG.18: VELOCITY AMPLIFICATION RATIO vs ROTATIONAL SPEED. COMPARISON OF SECOND ORDER THEORY WITH EXPERIMENTS

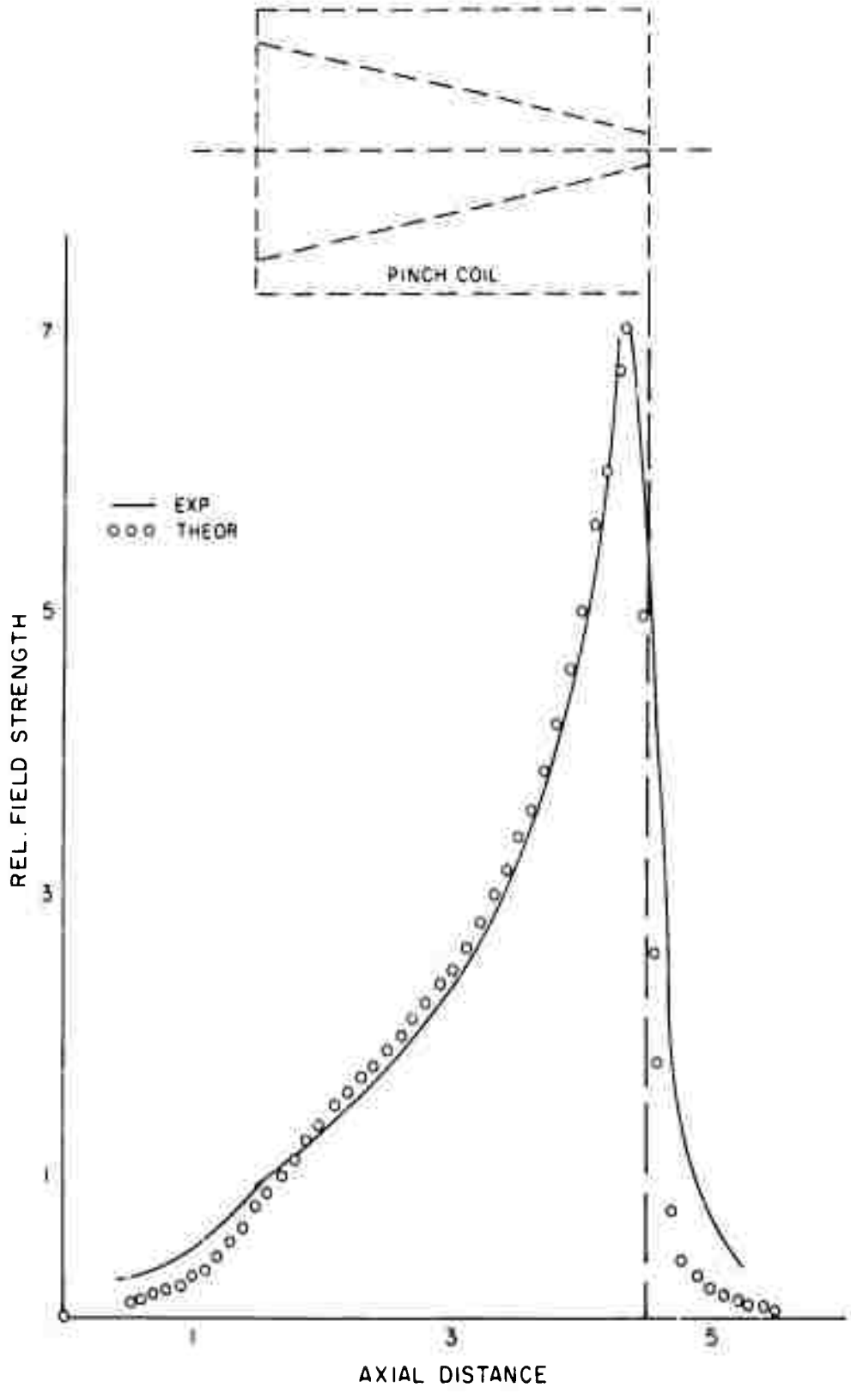

FIG. 19: DISTRIBUTION OF AXIAL MAGNETIC INDUCTION IN CONICAL COIL. COMPARISON BETWEEN THEORY AND MEASUREMENTS

APPENDIX

To calculate the magnetic induction on the axis of a conical coil due to an applied potential constant along its length, assume that the current is confined to a thin layer adjacent to the conical hole. This is justified for fairly high frequencies where the skin effect naturally restricts the depth of the current-carrying layer. Calling the distance of a point on the axis from the apex h, the distance of the near edge h_1 and that of the far end h_2, we can calculate the field induction along the cone axis B by integrating over all circular current loops of thickness dh_o carrying a current $i(h_o)$, thus:

$$B = (\mu/2) \int_{h_1}^{h_2} R^2 i(h_o)(R^2 + (h_o - h)^2)^{-3/2} dh_o \qquad (42)$$

where h_o is the axial position of the current loop, R is its radius and μ is the permeability of free space. If the apex angle of the cone is θ_o, we have:

$$\tan \theta_o = R/h_o$$

which allows elimination of R from (42). To estimate the functional dependence of $i(h_o)$ on h_o, we assume that the frequency of the applied potential is high enough to make the current distribution resistance dependent. Hence, if the applied voltage is independent of h_o, we have from Ohm's law:

$$i(h_o) = k/h_o$$

where k is a constant. Substituting this in (42) we obtain:

$$B = (\mu/2)k \int_{h_1}^{h_2} h_o(h_o^2 \sec^2\theta_o - 2hh_o + h^2)^{-3/2} \tan^2\theta_o \, dh_o$$

which is explicitely:

$$B = (\mu/2h)k \left[(h_1 - h)(h_1^2\sec^2\theta_o - 2hh_1 + h^2)^{-1/2} - (h_2 - h)(h_2^2\sec^2\theta_o - 2hh_2 + h^2)^{-1/2} \right] \qquad (43)$$

The course of the function B(h), (43) is shown in Figure 19. Comparison is made with measurements using a small magnetic probe consisting of a coil 1 mm diameter and 3 mm long mounted on a traversing rig. The coil was energized by a 3 Mhz signal generator matched into the load by a ferrite cored step-down transformer. The frequency of 3 Mhz was chosen to obtain adequate sensitivity of the probe, but variation of the frequency did not seem to cause material changes in the results. As k is an arbitrary constant, the theoretical and experimental curves were normalized at their peak.

Preceding page blank

As will be seen, the agreement is good over most of the length of the coil. A salient feature of the result is the rapid rise of the field strength toward the apex of the cone. When it is remembered that the magnetic pressure is proportional to the square of the field strength, the dependence of pressure on axial position will be a very steep function. Calculations show that this is one of the conditions under which a thin jet is produced by magnetic pressure and elastic contraction of the cone.